Wind-driven ocean dynamics impact on the contrasting sea-ice trends around West Antarctica

Article *in* Journal of Geophysical Research: Oceans · March 2017

DOI: 10.1002/2016JC012416

7 authors, including:

Sang-Ki Lee
National Oceanic and Atmospheric Administrat…
72 PUBLICATIONS **1,724** CITATIONS
SEE PROFILE

Denis L. Volkov
National Oceanic and Atmospheric Administrat…
46 PUBLICATIONS **451** CITATIONS
SEE PROFILE

Arnold L. Gordon
Columbia University
282 PUBLICATIONS **12,623** CITATIONS
SEE PROFILE

Yanyun Liu
University of Miami
18 PUBLICATIONS **182** CITATIONS
SEE PROFILE

Wind-driven ocean dynamics impact on the contrasting sea-ice trends around West Antarctica

Sang-Ki Lee[1], Denis L. Volkov[2,1], Hosmay Lopez[2,1], Woo Geun Cheon[3], Arnold L. Gordon[4], Yanyun Liu[2,1] and Rik Wanninkhof[1]

[1]Atlantic Oceanographic and Meteorological Laboratory, NOAA, Miami, FL

[2]Cooperative Institute for Marine and Atmospheric Studies, University of Miami, Miami, FL

[3]The 6th R&D Institute-1, Agency for Defense Development, Changwon, Republic of Korea

[4]Lamont-Doherty Earth Observatory, Earth Institute at Columbia University, Palisades, New York, USA

Submitted to Journal of Geophysical Research (Second Revision)

March 2017

Corresponding author address: Dr. Sang-Ki Lee, NOAA, Atlantic Oceanographic and Meteorological Laboratory, 4301 Rickenbacker Causeway, Miami, FL 33149, USA.

E-mail: Sang-Ki.Lee@noaa.gov.

Abstract

Since late 1978, Antarctic sea-ice extent in the East Pacific has retreated persistently over the Amundsen and Bellingshausen Seas in warm seasons, but expanded over the Ross and Amundsen Seas in cold seasons, while almost opposite seasonal trends have occurred in the Atlantic over the Weddell Sea. By using a surface-forced ocean and sea-ice coupled model, we show that regional wind-driven ocean dynamics played a key role in driving these trends. In the East Pacific, the strengthening Southern Hemisphere (SH) westerlies in the region enhanced the Ekman upwelling of warm upper Circumpolar Deep Water and increased the northward Ekman transport of cold Antarctic surface water. The associated surface ocean warming south of 68°S and the cooling north of 68°S directly contributed to the retreat of sea ice in warm seasons and the expansion in cold seasons, respectively. In the Atlantic, the poleward shifting SH westerlies in the region strengthened the northern branch of the Weddell Gyre, which in turn increased the meridional thermal gradient across it as constrained by the thermal wind balance. Ocean heat budget analysis further suggests that the strengthened northern branch of the Weddell Gyre acted as a barrier against the poleward ocean heat transport, and thus produced anomalous heat divergence within the Weddell Gyre and anomalous heat convergence north of the gyre. The associated cooling within the Weddell Gyre and the warming north of the gyre contributed to the expansion of sea ice in warm seasons and the retreat in cold seasons, respectively.

1. Introduction

The satellite passive microwave data record since late 1978 shows that the Antarctic sea-ice extent has overall expanded in all seasons [e.g., Turner and Overland, 2009], in stark contrast to the retreating Arctic sea-ice extent [e.g., Stroeve et al., 2012]. Several studies have suggested that the surface freshening and enhanced salinity stratification in the Antarctic seas, caused by the melting of the Antarctic glaciers and ice-sheet related to anthropogenic global warming, suppressed convective mixing with the warmer water at depth and thus inhibited the melting of Antarctic sea ice overall [e.g., Bintanja et al., 2015; de Lavergne et al., 2014; Bintanja et al., 2013; Zhang, 2007]. However, around West Antarctica, the trend is not homogeneous throughout the seasons or the longitudes [e.g., Parkinson and Cavalieri, 2012]. In particular, as shown in Figures 1a and b, Antarctic sea-ice extent in the East Pacific sector (150°W - 80°W) has retreated substantially over the Amundsen and Bellingshausen Seas during the warm seasons from December to May (DJFMAM), but expanded over the eastern Ross and Amundsen Seas during the cold seasons from June to November (JJASON) - the warm and cold seasons are defined based on the seasonality of Antarctic sea-ice extent. See Figure 2 for the names of the oceans and regional seas around Antarctica. In the Atlantic sector (60°W - 0°), on the other hand, the sea-ice extent has expanded over the Weddell Sea during the warm seasons, but retreated during the cold seasons.

Antarctic sea ice is intimately coupled to the atmosphere-ocean processes over the Southern Ocean. For example, the expansion and retreat of Antarctic sea ice exert a major control on surface albedo and thus the atmospheric radiative energy balance [e.g., Ebert and Curry, 1993; Walsh, 1983]. Antarctic sea ice insulates the underlying ocean from the air-sea fluxes of heat,

momentum and carbon. Therefore, its long-term trend could either slow down or accelerate ocean warming and acidification (see Wanninkhof et al. [2013] and Takahashi et al. [2009] for the global ocean carbon uptake, and Rysgaard et al. [2011] for the Antarctic sea-ice contribution to the air-sea CO_2 flux in the Southern Ocean), and thus potentially modulate the Southern Ocean's response to the increasing anthropogenic greenhouse gases. Additionally, Antarctic sea ice affects the availability of food and shelter for Antarctic krill (*Euphausia superba*), the key species in the Antarctic marine food web, during the early life stages and thus impacts their survival [e.g., Piñones and Fedorov, 2016; Brierley et al., 2002; Meyer et al., 2002].

Various hypotheses have been proposed to explain the spatially and seasonally inhomogeneous trend of sea-ice extent around West Antarctica. Several studies have suggested that the positive trend of the Southern Annular Mode (SAM) during the past decades (due to ozone depletion and increasing greenhouse gases) and El Niño-Southern Oscillation (ENSO) teleconnections are mainly responsible for the observed sea-ice trends through their influences on wind-driven surface heat flux [Matear et al., 2015; Ding et al., 2011; Stammerjohn et al., 2008; Yuan and Li, 2008; Liu et al., 2004; Yuan, 2004; Kwok and Comiso, 2002; Renwick, 2002]. Many of these studies also pointed out that wind-driven surface heat flux alone is insufficient to explain the magnitude and the spatiotemporal pattern of the observed Antarctic sea-ice trend [e.g., Liu et al., 2004]. For instance, Holland and Kwok [2012] argued that wind-driven changes in sea-ice drift are the main driver of the sea-ice trends around West Antarctica during 1992 - 2010, while Matear et al. [2015] suggested that anthropogenic warming is required to explain the observed sea-ice retreat in the Amundsen and Bellingshausen Seas since 1979.

Clem and Renwick [2015] suggested that the increasing tendency of atmospheric convection over the South Pacific Convergence Zone forced stationary Rossby waves to strengthen the Southern Hemisphere (SH) subpolar low over West Antarctica, which in turn could bring cold Antarctic air northward over the East Pacific sector and warm subtropical air southward over the Atlantic sector. This hypothesis is indeed consistent with the increasing Antarctic sea-ice concentration in the East Pacific sector and the decreasing Antarctic sea-ice concentration in the Atlantic sector during the cold seasons (Figure 1b), although it does not explain the opposite trends during the warm seasons (Figure 1a). Meehl et al. [2016] proposed a similar hypothesis suggesting that the increasing Antarctic sea-ice extent during 2000 - 2014, the period known as the global warming hiatus [e.g., Meehl et al., 2011], is linked to the negative phase of the Interdecadal Pacific Oscillation (IPO). Purich et al. [2016] used coupled model simulations to present a result consistent with Meehl et al. [2016]. They stressed that the phase change in the IPO from positive to negative over 1979-2013 contributed to the observed strengthening of the SH subpolar low over the Amundsen Sea and the associated cold- and warm-air advections, thereby increasing the sea ice in the Ross Sea and decreasing it in the Bellingshausen Sea. Founded on a similar mechanism, Li et al. [2014] proposed that warm tropical North Atlantic sea surface temperatures (SSTs), associated with the Atlantic Multidecadal Oscillation (AMO) [Enfield et al., 2001], could produce interhemispheric teleconnections [Ji et al., 2014; Simpkins et al., 2014; Lee et al., 2013; Wang et al., 2010] to strengthen the SH subpolar low over the Amundsen Sea. Zhang et al. [2016], using a fully coupled climate model, also reported that North Atlantic SSTs could influence the changes in Antarctic sea-ice extent emphasizing the Atlantic Meridional Overturning Circulation as the main driver.

Previous studies, as discussed above, have collectively shown that changes in local winds, induced by the positive trend of SAM and stationary Rossby waves emanating from the tropical Pacific and Atlantic, together with a warming-induced surface freshening, caused the spatially and seasonally inhomogeneous sea-ice trend around West Antarctica. They stressed wind-driven surface heat fluxes (i.e., warm- and cold-air advections) and sea-ice transport, and enhanced salinity stratification, as the key forcing mechanisms. However, in many of these studies the potential role of wind-driven ocean dynamics was either neglected or not fully incorporated, partly due to the scarcity of in-situ ocean observations in the Antarctic seas [e.g., Legler et al., 2015; Rintoul et al., 2012]. Since both atmosphere and ocean processes are involved in the seasonal formation and melting of Antarctic sea ice [e.g., Gordon and Taylor, 1975], it is likely that regional ocean dynamics played an important role in shaping the spatially and seasonally inhomogeneous sea-ice trend around West Antarctica. Therefore, our main goal in this study is to investigate if and how the recent trends of West Antarctic sea ice were affected by regional ocean dynamics. To achieve this goal, we utilize satellite-derived sea-ice data and a surface-forced ocean and sea-ice coupled model.

Section 2 describes the observational data, the model, and the model experiments that were utilized. Section 3 shows the modeled sea-ice trends around West Antarctica and compares them with the observations. The model results for the East Pacific (150°W - 80°W) and Atlantic (60°W - 0°) sectors are analyzed in section 4 and 5, respectively. Based on these analyses, we present (1) Ekman heat transport and upwelling, and (2) the spin-up of the Weddell Gyre as the key contributing factors to the inhomogeneous sea-ice trends around West Antarctica. Section 6 further presents and discusses the interannual variability of Antarctic sea ice around West

Antarctica by using the leading Empirical Orthogonal Function (EOF) modes of detrended Antarctic sea-ice variability. Section 7 provides a summary and discussion.

2. Data and Model Experiments

The Hadley Center sea ice and SST data sets [Rayner et al., 2003] were used to derive monthly observed sea-ice concentration data for the period of 1979 - 2014. The monthly sea-ice concentration data were reconstructed by blending and adjusting all available digitized sea-ice data including the passive microwave satellite data from late 1978 onward measured from several sensors [Rayner et al., 2003]. There is no reliable long-term in-situ ocean observation system in place in the Antarctic seas [Legler et al., 2015; Rintoul et al., 2012]. Therefore, we used the ocean and sea-ice model components of the NCAR Community Earth System Model version 1 (CESM1; Danabasoglu et al., 2012) forced with the Modern-Era Retrospective analysis for Research and Applications (MERRA; Rienecker et al., 2011) surface flux fields for the period of 1979 - 2014 in order to reproduce the observed Antarctic sea-ice trends and to further explore the role of ocean dynamics.

The ocean component of CESM1 is based on the Parallel Ocean Program version 2, [Danabasoglu et al., 2012]. The sea-ice component of CESM1 is based on the Community Ice Code version 4, which is a dynamic-thermodynamic sea-ice model that treats the ice pack as a flow-dependent elastic-viscous-plastic material [Hunke and Lipscomb, 2008]. The ocean model is divided into 60 vertical levels. Both the ocean and sea-ice model components have 360 longitudes and 384 latitudes on a displaced pole grid, with a longitudinal resolution of about 1.0° and a variable latitudinal resolution of approximately 0.3° near the equator and about 1.0°

elsewhere. An important advancement in CESM1 from earlier versions is the specification of a spatially variable coefficient in the Gent and McWilliams eddy parameterization, rather than a constant value; the ocean response (e.g., strengthening of the Antarctic Circumpolar Current) to increasing SH winds is in reasonable agreement with experiments using ocean models with much higher resolution that do not use this eddy parameterization [Gent and Danabasoglu, 2011]. Danabasoglu et al. [2012] provide a more detailed description of the CESM1 ocean model. See Landrum et al. [2012] for the simulation of Antarctic sea-ice climatology in the fully coupled CESM1.

To spin up the CESM1 ocean and sea-ice model, it was initialized using temperature and salinity fields obtained from the polar hydrographic climatology [Steele et al., 2001] and integrated for 400 years using the 20th century reanalysis (20CR) surface flux fields from the period of 1948 - 1977 [Compo et al., 2011]. In the spin-up run, the 6-hourly surface wind vectors, air temperature and specific humidity, daily shortwave and downward longwave radiative heat fluxes, and monthly precipitation rate were specified. The upward longwave radiative heat flux and turbulent surface fluxes were determined interactively by using the 6-hourly surface wind speed, air temperature and specific humidity, along with the model-produced SSTs. During the spin-up, the surface flux fields in each model year were randomly selected from the period of 1948 - 1977, following the time-shuffling spin-up method used in Lee et al. [2011] and others [e.g., Liu et al., 2015; Lee et al., 2015]. By using this spin-up method, the impact of atmospheric noise, which is crucial especially for sustaining thermohaline convection and deep-water formation in the North Atlantic sinking regions [e.g., Wu et al., 2016; Kirtman et al., 2012], can be retained while minimizing any spectral peaks in the surface flux fields at interannual and longer time scales. In

185 the spin-up run and also in other runs, the long-term mean values of freshwater discharge from
186 continents, derived from Dai and Trenberth [2002], were prescribed. A constant freshwater flux
187 of 0.073 Sv (10^6 m^3 s^{-1}), which was derived based on a freshwater flux budget of the Southern
188 Ocean [Large and Yeager, 2009], was uniformly distributed along the Antarctic coast - Jacobs et
189 al. [1992] estimated a slightly larger value of 0.083 Sv based on direct observations. In addition,
190 the global sea surface salinity fields were slowly relaxed (i.e., freshwater flux of 0.994 mm day^{-1}
191 per psu) to the polar hydrographic climatology to prevent the model salinity fields from drifting
192 away from the observed climatology.
193
194 After the 400 years of the spin-up run, the 20CR surface flux fields were used to force the
195 CESM1 ocean and sea-ice model continuously for the period of 1948 - 1978, while the MERRA
196 surface flux fields were used to continue the model run for 1979 - 2014. Note that the 20CR
197 surface flux fields were corrected by using the surface flux fields obtained from the common
198 ocean–ice reference experiments (CORE) version 2 [Large and Yeager, 2009] (see Text S1 in the
199 supporting information for detail). Additionally, to ensure a smooth transition of the model
200 simulation during the late 1970s, the MERRA climatological surface flux fields were adjusted to
201 match the corrected 20CR climatological surface flux fields (see Text S2 in the supporting
202 information for detail). The 36-year CESM1 ocean and sea-ice model simulation forced with the
203 adjusted MERRA surface flux fields is referred to as the historical simulation. Additionally, the
204 spin-up run was continued for additional 600 years, which is referred to as the reference
205 simulation and utilized to carry out a heat budget analysis.
206

3. West Antarctic Sea-Ice Trends in Historical Simulation

The linear trends in Antarctic sea-ice concentration over the period of 1985 - 2014 for the warm and cold seasons obtained from the historical simulation are shown in Figures 1c and d, respectively. Note that the first six years (1979 - 1984) of the model results were excluded to prevent any potential model drift in the beginning of the historical simulation from affecting the modeled sea-ice trend. Overall, the historical simulation reproduced the spatial patterns of sea-ice trend around West Antarctica for both the warm and cold seasons reasonably well (Figures 1a and b), such as the largely decreasing Antarctic sea-ice concentration over the East Pacific sector in the warm seasons and over the Atlantic sector in the cold seasons, although there are considerable differences between the historical simulation and the observations in other regions especially over the West Pacific. Since the linear trends of West Antarctic sea-ice concentration are regionally coherent within the East Pacific sector (150°W - 80°W) and within the Atlantic sector (60°W - 0°), and reasonably well reproduced in the historical simulation, the linear trends of West Antarctic sea-ice concentration are zonally averaged and explored for each of the regions in the following sections. As shown in Figures S1 - S4 in the supporting information, the climatological ocean temperature and salinity fields in the East Pacific and Atlantic sectors derived from the historical simulation are generally in good agreement with those from an optimally interpolated in situ dataset.

4. Antarctic Sea-Ice Trend in the East Pacific Sector

Figures 3a and b show the linear trends of Antarctic sea-ice concentration averaged over the East Pacific sector for each calendar month obtained from the historical simulation and the observations, respectively. The two green lines in each panel represent the 5% and 90%

climatological sea-ice concentration boundaries. Hereafter, the area between the 5 and 90% sea-ice concentration boundaries is referred to as the marginal ice zone, while the area with greater than 90% sea-ice concentration as the interior of the ice pack. Although the historical simulation underestimates the decreasing sea-ice concentration in the warm seasons and overestimates the increasing sea-ice concentration in the cold seasons, the model reproduced the overall spatiotemporal pattern of Antarctic sea-ice trend in the East Pacific sector reasonably well. It should be noted that the changes in Antarctic sea-ice concentration over the East Pacific sector during the recent decades occurred mainly in the marginal ice zone, while the interior of the ice pack that mainly forms in the cold seasons was nearly unaffected.

To address if and how ocean dynamics affected the seasonally distinctive Antarctic sea-ice trends over the marginal ice zone in the East Pacific sector, we first investigate the linear trends of ocean temperature zonally averaged over the East Pacific sector. As shown in Figures 4c and d, the upper ocean temperatures north of 68°S decreased considerably (up to -1.0°C) in both the cold and warm seasons, the former being in line with the increasing sea-ice concentration in the marginal ice zone (Figure 4b). As shown in Figure 5b, the year-round cooling trends of the upper ocean north of 68°S (Figures 4c and d) are largely driven by the increasing northward advection of cold Antarctic surface water (see Talley et al. [2011] for the water mass distribution in the Southern Ocean). The increasing northward velocity in the upper 100 m is consistent with the overall positive trends of zonal wind stress (τ_x) and the implied Ekman transport. This suggests that the increasing northward advection of cold Antarctic surface water is driven by the increasing SH westerlies over the East Pacific sector enabled by the strengthening SH subtropical high and SH subpolar low in the region (Figures 6a, b and 7a; see Figures S5a and b

253 in the supporting information for the climatological sea level pressure and surface wind stress
254 vectors).
255
256 Perhaps, the most striking feature of the ocean temperature trends in the East Pacific sector
257 (Figures 4c and d) is the large warming of subsurface water between 100 and 400 m (up to
258 0.9°C). The subsurface warming is largely due to the enhanced regional upwelling of the warm
259 upper Circumpolar Deep Water (CDW) - the climatological ocean temperatures are warmer with
260 depth in this region because the upper ocean is relatively fresh and exposed to cold Antarctic air.
261 Indeed, as shown in Figure 5a, the marginal ice zone is exposed to the year-long Ekman
262 upwelling trend, induced by the negative wind stress curl tendency associated with the increasing
263 SH westerlies over the East Pacific sector (Figures 6a, b and 7a). The subsurface warming and
264 the concurrent decrease in the sea ice south of 68°S in the warm seasons (see Figures 4a and c)
265 suggest that the warm upper CDW is responsible for (or at least contributed to) the melting sea
266 ice in the warm seasons, in particular during austral fall in March - May (MAM) when the
267 surface mixed layer deepens. More specifically, the seasonal cooling at the surface and
268 seasonally enhanced vertical mixing (i.e., diffusion and convection) in austral fall entrain the
269 warm upper CDW to increase the mixed layer temperature and thus slow down (or disrupt) the
270 seasonal formation of sea ice. In austral spring and summer, the surface layer is too stratified and
271 stable to entrain the warm upper CDW to the surface.
272
273 The subsurface warming also prevails during the cold seasons (Figure 3d). However, it has little
274 impact on the sea-ice interior because the surface water in the interior away from coastal
275 polynyas is almost completely insulated from cold Antarctic air during the cold seasons; this

strongly inhibits vertical mixing, and thus reduces the warm upper CDW flux into the surface water. Consistent with this reasoning, the surface ocean temperatures south of 68°S did not change appreciably in the cold seasons (Figure 4d).

The above analysis suggests that the enhanced Ekman upwelling of the warm upper CDW and the increased northward cold water transport in the East Pacific sector, driven by the increasing SH westerlies in the region, changed the surface ocean temperatures in the marginal ice zone and thus the sea-ice concentration. However, air-sea heat flux could also affect the surface ocean temperatures in the marginal ice zone and thus the sea-ice concentration, and be affected by the changing sea-ice concentration. Therefore, in order to determine the causality of the sea-ice trends, it is necessary to carry out a heat budget analysis of the upper ocean. As summarized in equation (1) in Lee et al. (2007), vertical integration of the ocean heat conservation equation from the sea surface to a given depth yields an upper ocean heat balance among heat storage rate (Q_{STR}), advective heat flux (Q_{ADV}), net air-sea heat flux (Q_{SHF}), and other heat flux terms including horizontal and vertical diffusive heat fluxes, and penetrative shortwave heat flux at the base. The diffusive heat fluxes, which are parameterized in the CESM1 ocean model, are inferred from the residual heat flux (i.e., $Q_{RES} = Q_{STR} - Q_{ADV} - Q_{SHF}$) assuming that other terms such as the penetrative shortwave heat flux are relatively small. Note that the heat flux associated with ice formation and meting is included in the net air-sea heat flux (Q_{SHF}) for simplicity.

Figure 5c shows anomalies of advective heat flux (ΔQ_{ADV}), storage rate (ΔQ_{STR}), and residual heat flux (ΔQ_{RES}) in the upper 100 m, and net air-sea heat flux (ΔQ_{SHF}) averaged in the 80°S - 70°S and 68°S - 60°S latitude bands over the East Pacific sector. These heat flux anomalies are

299 computed from the historical simulation (the averages for the 1985 - 2014 periods) relative to the
300 reference simulation (the averages for 600 years). Figure 5c shows that the 75°S - 70°S latitude
301 band in the East Pacific sector is subject to anomalous advective heat convergence ($\Delta Q_{ADV} > 0$)
302 and warming tendency due to anomalous residual flux ($\Delta Q_{RES} > 0$). If it is assumed that the
303 residual flux largely represents vertical heat diffusion, this result is quite consistent with the
304 above conclusion that the enhanced Ekman upwelling of the warm upper CDW and the vertical
305 mixing slowed down (or disrupted) the seasonal formation of sea ice during the warm seasons.
306 The warming tendencies due to the anomalous advective heat convergence and residual heat flux
307 are largely compensated by the negative air-sea heat flux anomaly ($\Delta Q_{SHF} < 0$). This suggests
308 that the air-sea heat flux is not the cause of the decreased sea-ice concentration in the warm
309 seasons. It is more likely that the negative air-sea heat flux anomaly is a response because the
310 decreased sea-ice concentration enlarged the area of the surface water in contact with cold
311 Antarctic air.
312
313 Figure 5c shows that the 68°S - 60°S latitude band is also affected by anomalous advective heat
314 divergence ($\Delta Q_{ADV} < 0$), which is consistent with the above conclusion that the increased
315 northward transport of cold Antarctic surface water enhanced the sea-ice concentration in the
316 cold seasons. The anomalous advective heat divergence is largely compensated by the warming
317 tendency due to the anomalous residual heat flux ($\Delta Q_{RES} > 0$). Assuming that the residual flux to
318 a large extent represents vertical heat diffusion and convection, this suggests that the vertical
319 mixing with the warm upper CDW nearly compensates the cooling tendency associated with the
320 anomalous advective heat divergence. The anomalous air-sea heat flux is relatively small and

positive, and thus represents a response rather than a driver because the increased sea-ice concentration reduced the area of the surface water in contact with cold Antarctic air.

5. Antarctic Sea-Ice Trend in the Atlantic Sector

As indicated in Figures 3c and d, the interior of the ice pack in the Weddell Sea is almost unaffected, in agreement with the earlier reports that the Weddell Polynya of the mid-1970s has not reemerged since [e.g., Gordon et al., 2007; Cheon et al., 2015]. More importantly, the seasonality of the Antarctic sea-ice trend in the Atlantic sector is almost perfectly opposite to that in the East Pacific sector (Figures 3a and b). The upper ocean temperatures became colder (up to -0.6°C) over the marginal ice zone in the warm seasons (Figure 8c) consistent with the increasing sea-ice concentration (Figure 8a). Similar to the East Pacific sector, a large warming occurred below the surface (up to 0.7°C) north of around 65°S. However, it appears that the subsurface warming has little impact on the upper ocean temperatures during the warm seasons, in contrast to the East Pacific sector.

As shown in Figure 6a, the SH westerlies increased south of about 50°S over the Atlantic sector during the warm seasons due to the strengthening of the SH subpolar low over the Antarctic Peninsula and SH subtropical high over the Atlantic sector (see Figure S5a in the supporting information for the climatological sea level pressure and surface wind stress vectors during the warm seasons). Due to this poleward intensification of the SH westerlies in the Atlantic sector [e.g., Lee and Feldstein, 2013; Thompson and Solomon, 2002], the northward velocity in the upper 100 m increased during the warm seasons (Figure 9b), which coincides with the cooler upper ocean temperatures and the increasing sea-ice concentration north of around 65°S over the

marginal ice zone (Figures 8a and c). However, the northward velocity in the upper 100 m did not increase south of 65°S, and thus cannot explain the cooler upper ocean temperatures or the increased sea-ice concentration south of 65°S.

During the cold seasons, the upper ocean temperatures in the marginal ice zone are much warmer (up to 0.7°C) especially north of 60°S (Figure 8d) in line with the decreasing sea-ice concentration (Figure 8b). As shown in Figures 6b and 9b, the SH westerlies over the Atlantic sector north of 64°S weakened considerably during the cold seasons due to the weakening SH subpolar low over the Atlantic and Indian sectors (see Figure S5b in the supporting information for the climatological sea level pressure and surface wind stress vectors during the cold seasons), which could be traced back to atmospheric convection in the tropical Atlantic [Simpkins et al., 2014; Lee et al., 2013] and Indian summer monsoon regions [Lee et al., 2013]. The weakening SH westerlies in the Atlantic sector sharply reduced the northward Ekman transport, which in turn resulted in an anomalous southward Ekman transport of warmer surface water. Therefore, it is likely that the anomalous southward Ekman transport of warm surface water contributed to the retreat of sea-ice extent over the Atlantic sector in the cold seasons.

It is clear from the above discussion that Ekman dynamics are not sufficient to explain the seasonality of Antarctic sea-ice trend in the Atlantic sector, particularly the increasing sea-ice concentration in the Weddell Sea during the warm seasons. Nevertheless, the upper ocean heat budget (Figure 9c) indicates that the surface 100 m water in the Weddell Sea south of 68°S is affected by anomalous advective heat divergence ($\Delta Q_{\mathrm{ADV}} < 0$). Therefore, there must be an alternative way that ocean dynamics affected the seasonality of Antarctic sea-ice trend in the

Atlantic sector, while other mechanisms such as sea-ice transport and cold- and warm-air advections could also contribute. Unlike the East Pacific sector, the ocean temperature changes in the Atlantic sector are not limited to the upper few hundred meters, but extend down to 2000 m or even deeper (Figures 8c and d). The ocean temperatures in the upper 2000 m over the Atlantic sector decreased south of 65°S ~ 58°S and increased north of 65°S ~ 58°S, producing a sharp anomalous meridional thermal gradient. Constrained by the thermal wind relationship, the northern branch of the Weddell Gyre strengthened across the increased meridional thermal gradient between 65°S and 55°S (Figures 8e and f).

The large increases in the eastward-flowing branch of the Weddell Gyre and the associated meridional thermal gradient indicate that the Weddell Sea is in a geostrophic equilibrium with the poleward shifting SH westerlies in the region, resulted from the poleward intensification of the SH westerlies in the warm seasons and the weakening in the cold seasons (Figures 6a, b and 7b) [e.g., Lee and Feldstein, 2013; Thompson and Solomon, 2002]. Note that the poleward shifting SH westerlies should produce negative wind stress curl anomalies south of 65°S and overall positive wind stress curl anomalies north of 65°S (Figure 7b). Due to the implied Ekman divergence south of 65°S and convergence north of 65°S, the meridional pressure gradient and the associated geostrophic zonal flow (i.e., the northern branch of the Weddell Gyre) should increase. Therefore, we hypothesize that the poleward shifting SH westerlies increased the northern branch of the Weddell Gyre and the associated meridional thermal gradient, and thus led to the cooler ocean temperatures within the Weddell gyre and the warmer ocean temperatures north of the gyre. This hypothesis is consistent with the expansion of sea ice south of 60°S in the warm seasons and the retreat north of 65°S in the cold seasons (Figures 8a and b).

Figure 10a further shows the upper 3000 m ocean heat budget terms within the Weddell Gyre (80°S - 66°S) and north of the gyre (62°S - 54°S) obtained from the reference simulation (the averages for 600 years). Their changes (or anomalies) during the 1985 - 2014 periods, obtained from the historical simulation (the averages for the 1985 - 2014 periods) relative to the reference simulation (the averages for 600 years), are also shown in Figure 10b. As shown in Figure 10a, the Weddell Sea south of 68°S releases heat to the atmosphere at a rate of -9.9 Wm^{-2} (positive downward), which is compensated by advective heat convergence (Q_{ADV} ~ 5.4 W m^{-2}) and warming tendency due to residual flux (Q_{RES} ~ 4.5 W m^{-2}). During 1985 - 2014, the advective heat convergence decreased by about 50%, which is largely responsible for cooling the water column within the Weddell Gyre (Figure 9b). In the reference simulation (Figure 10a), the 62°S - 52°S latitude band north of the Weddell Gyre is subject to advective heat convergence (Q_{ADV} ~ 26.5 W m^{-2}), which is compensated by negative air-sea heat flux (Q_{SHF} ~ -4.9 W m^{-2}) and cooling tendency due to residual heat flux (Q_{RES} ~ -21.6 W m^{-2}). The advective heat convergence increased ($\Delta Q_{ADV} > 0$) during 1985 - 2014, which is solely responsible for warming the water column north of the Weddell Gyre (Figure 10b).

The above heat budget analysis strongly suggests that the strengthened northern branch of the Weddell Gyre acted as a barrier against the poleward ocean heat transport into the Weddell Sea, and thus produced anomalous advective heat divergence ($\Delta Q_{ADV} < 0$) within the Weddell Gyre and anomalous advective heat convergence ($\Delta Q_{ADV} > 0$) north of the gyre. This hypothesis provides an important physical mechanism that links the wind-driven spin-up of the Weddell

Gyre and the anomalous meridional thermal gradient that formed across the northern branch of the gyre (Figures 8c - f).

It appears that the anomalous advective heat divergence ($\Delta Q_{ADV} < 0$) within the Weddell Gyre and the anomalous advective convergence ($\Delta Q_{ADV} > 0$) north of the gyre directly influenced the upper 100 m ocean heat budget (see Figures 9c and 10b). Additionally, the cooling and warming in the deeper ocean could also influence the upper 100 m ocean heat budget through vertical mixing. This argument is supported by the cooling tendency of the anomalous residual heat flux ($\Delta Q_{RES} < 0$) within the Weddell Gyre and the warming tendency of the anomalous residual heat flux ($\Delta Q_{RES} > 0$) north of the gyre (Figure 9c).

6. Interannual Variability of West Antarctic Sea Ice

Our analysis indicates that the increasing SH westerlies in the East Pacific sector and the poleward shifting SH westerlies in the Atlantic sector contributed to the seasonally and spatially inhomogeneous sea-ice trends around West Antarctica during the past decades. These trends in the SH westerlies are known to be linked to ozone depletion and increasing greenhouse gases [e.g., Lee and Feldstein, 2013; Son et al., 2008; Shindell and Schmidt, 2004; Gillett and Thompson, 2003], and the phase changes in the IPO and AMO [e.g., Lopez et al., 2016; Meehl et al., 2016; Purich et al., 2016; Zhang et al., 2016; Simpkins et al., 2014; Lee et al., 2013]. However, the trends in the SH westerlies could also emerge from the residuals of local and remotely forced atmospheric modes of variability from synoptic to interannual time scales, such as the SAM [e.g, Limpasuvan and Hartmann, 1999; Domingues et al., 2014], the Pacific-South American patterns [Mo and Higgins, 1998; Lau et al., 1994; Ghil and Mo, 1991] and ENSO-

435 forced extratropical Rossby waves. In particular, the SAM is largely intrinsic atmospheric
436 variability with e-folding time (or de-correlation time) of up to 20 days in the warm seasons and
437 less than 10 days in the cold seasons below the tropopause [e.g., Baldwin et al., 2003]. This
438 suggests a possibility that the long-term trends in Antarctic sea-ice extent are the footprint of
439 decadal changes in the frequency and amplitude of interannual Antarctic sea-ice variability.
440
441 Figures 11a and b show the leading EOF modes of detrended Antarctic sea-ice variability for the
442 warm and cold seasons, respectively, derived from the observations. The leading EOF modes
443 show a contrasting pattern of spatial and seasonal sea-ice variations around West Antarctica,
444 which is surprisingly similar to the spatiotemporal pattern of the linear trends (see Figures 1a and
445 b). Interestingly, the leading EOF modes of detrended sea-ice variability around East Antarctica
446 are relatively weak. The leading EOF modes derived from the historical simulation (Figures 11c
447 and d) are quite consistent with those from the observations. The principal components (PCs) of
448 the leading EOF modes are also highly correlated between the observations and the historical
449 simulation (Figures 11e and f).
450
451 The apparent similarity between the leading modes of detrended Antarctic sea-ice variability and
452 the linear trends indeed suggests that the linear trends and interannual variability in West
453 Antarctic sea ice are affected by similar wind-driven ocean dynamics, although it is likely that
454 meridional Ekman heat transport plays a more important role at interannual time scale than other
455 slow ocean processes that involve subsurface and deeper waters [Ferreira et al., 2015]. However,
456 the leading EOF modes explain only about 20% of the total variance (Figures 11e and f).
457 Therefore, higher EOF modes should be also investigated to better understand the interannual

variability of West Antarctic sea ice and the role of wind-driven ocean dynamics versus other potentially important mechanisms identified in previous studies. Such a comprehensive analysis of interannual variability in West Antarctic sea ice is a subject of future study.

7. Summary and Discussion

We investigated the potential role of wind-driven ocean dynamics in the spatially and seasonally inhomogeneous sea-ice trends around West Antarctica during the recent decades, using a surface-forced ocean and sea-ice coupled model that reasonably reproduces these trends. Our analysis of the model simulation shows that wind-driven ocean dynamics played a crucial role in the summer-fall retreat and winter-spring expansion of Antarctic sea-ice extent in the East Pacific sector (150°W - 80°W) during the recent decades. As summarized in Figure 12a, the enhanced Ekman upwelling of the warm upper CDW followed by vertical mixing directly contributed to the summer-fall retreat of Antarctic sea-ice extent over the Amundsen and Bellingshausen Seas, while the increased northward Ekman transport of cold Antarctic surface water contributed to the winter-spring expansion over the eastern Ross and Amundsen Seas. Both the enhanced upwelling and northward transport were driven by the increasing SH westerlies over the East Pacific sector.

The linear trends of Antarctic sea ice in the Atlantic sector (60°W - 0°) are also strongly affected by wind-driven ocean dynamics. Ekman dynamics still played an active role in the Atlantic sector particularly in the retreat of sea ice during the cold seasons. However, the way in which wind-driven ocean dynamics affected the sea-ice trend is quite different in this region. As summarized in Figure 12b, the poleward shifting SH westerlies in the Atlantic sector

481 strengthened the eastward-flowing northern branch of the Weddell Gyre. Constrained by the
482 thermal wind relationship, the meridional thermal gradient increased sharply across the northern
483 boundary of the gyre. It appears that the strengthened northern branch of the Weddell Gyre acted
484 as a barrier against the poleward ocean heat transport, and thus produced anomalous heat
485 divergence within the Weddell Gyre and anomalous heat convergence north of the gyre. The
486 associated cooling of the water column within the Weddell Gyre therefore led to higher sea-ice
487 concentration in the warm seasons, while the warming of the water column north of the gyre
488 resulted in a retreat of sea-ice extent in the cold seasons.
489
490 Although not discussed in this study, we conducted an additional CESM1 ocean and sea-ice
491 model simulation using the European Centre for Medium-Range Weather Forecasts - Interim
492 (ERA-Interim) surface flux fields [Dee et al., 2011], and another ocean and sea-ice coupled
493 model simulation using the Modular Ocean Model version 5 [Griffies, 2012] with the ERA-
494 Interim surface flux fields. These two additional simulations with different sets of models and
495 surface flux fields provided results that are overall consistent with those presented in this study
496 indicating that our conclusions are not restricted to our particular choice of model and surface
497 flux fields. Nevertheless, it is important to point out some of the limitations in this study. In
498 particular, as discussed in section 2, a constant value of freshwater flux was uniformly
499 distributed along the Antarctic coast in the model simulations. However, recent studies showed
500 that approximately half of the melting water comes from small, warm-cavity ice shelves in the
501 East Pacific sector occupying only a small fraction of the total Antarctic ice-shelf area [e.g.,
502 Rignot et al, 2013]. Additionally, the global sea surface salinity fields, including those in the
503 Antarctic seas, were slowly relaxed to the monthly climatological fields to prevent the model

salinity fields from drifting away from the observed climatology. Such treatments of the freshwater discharge and sea surface salinity fields could limit the model's ability to simulate the increasing salinity stratification in the Antarctic seas and its impact on Antarctic sea ice. It is quite possible that the model's inability to simulate the large Antarctic sea-ice gain in the West Pacific is linked to this limitation in the CESM1 ocean and sea-ice model.

The results presented in this study leave open some important scientific questions, which deserve future investigation. Most importantly, the wind-driven ocean dynamics identified in this study should work in concert with various other mechanisms identified in earlier studies, particularly wind-driven sea-ice transport [Holland and Kwok, 2012] and cold- and warm-air advections linked to the IPO, AMO and SAM [Purich et al., 2016; Meehl et al. 2016; Clem and Renwick, 2015; Li et al., 2014] and warming-induced surface freshening [e.g., Bintanja et al., 2015; de Lavergne et al., 2014; Bintanja et al., 2013; Zhang, 2007]. A more consistent and thorough mechanism will emerge when all the key factors and their interactions are considered together.

Finally, the new findings reported in this study support the ongoing international efforts to implement a sustained in-situ ocean observation system in the Southern Ocean including the Antarctic seas [Russell et al., 2014; Rintoul et al., 2012]. Since standard Argo floats are hindered from transmitting data under sea ice, alternative observation platforms suitable for sub-ice ocean profile measurement, such as ice-tethered profilers, underwater gliders and polar profiling floats [Abrahamsen, 2014] are being tested and used to augment the existing ocean observation systems such as the repeated high-density Expendable Bathythermographs (XBT) transects along AX22, AX25, and IX28. Establishing a sustained in-situ ocean observation system in the

Antarctic seas will increase our ability to better monitor and predict future changes in Antarctic sea ice and their far reaching impacts on the global thermohaline ocean circulation [e.g., Abernathey et al., 2016], deep water formation and warming in the Southern Ocean [e.g., Cheon et al., 2015; de Lavergne et al., 2014; Gordon, 2014], the global carbon cycles [e.g., Rysgaard et al., 2011], and the Antarctic marine ecosystem [e.g., Brierley et al., 2002].

Acknowledgments

We would like to sincerely thank two anonymous reviewers for their thorough reviews and thoughtful comments and suggestions, which led to a significant improvement of the paper. S.-K. Lee acknowledges Steven Yeager for useful discussions on the CESM1 model simulations, Greg Foltz for helpful comments and suggestions, and Libby Johns for proofreading the manuscript. The Hadley Center sea ice and SST data sets were provided by UK Met Office at http://www.metoffice.gov.uk/hadobs/hadisst, 20CR and MERRA surface flux data sets were, respectively, provided by NOAA/ESRL/PSD at http://www.esrl.noaa.gov/psd, and by NASA/GSFC/GMAO at http://gmao.gsfc.nasa.gov/reanalysis/MERRA. This work was supported by NOAA's Climate Program Office, Climate Variability and Predictability Program (award GC16-207), and NOAA's Atlantic Oceanographic and Meteorological Laboratory. A. L. Gordon acknowledges support provided under the CICAR award number NA08OAR4320754 from NOAA. Lamont-Doherty Earth Observatory contribution number xxxx.

References

Abernathey, R. P., I. Cerovecki, P. R. Holland, E. Newsom, M. Mazloff, and L. D. Talley (2016), Water-mass transformation by sea ice in the upper branch of the Southern Ocean overturning, *Nat. Geosci*., doi:10.1038/ngeo2749.

Abrahamsen, E. P. (2014), Sustaining observations in the polar oceans, *Philos. Trans. Roy. Soc. London Ser. A, 372*, 20130337, doi:10.1098/rsta.2013.0337.

Baldwin, M. P., D. B. Stephenson, D. W. Thompson, T. J. Dunkerton, A. J. Charlton, and A. O'Neill (2003), Stratospheric memory and skill of extended-range weather forecasts. *Science, 301*, 636-640.

Bintanja, R., G. J. Van Oldenborgh, S. S. Drijfhout, B. Wouters, and C. A. Katsman (2013), Important role for ocean warming and increased ice-shelf melt in Antarctic sea-ice expansion, *Nat. Geosci*., *6*, 376-379.

Bintanja, R., G. J. Van Oldenborgh, and C. A. Katsman (2015), The effect of increased fresh water from Antarctic ice shelves on future trends in Antarctic sea ice, *Ann. Glaciol*., *56*, 120-126.

Brierley, A. S., P. G. Fernandes, M. A. Brandon, F. Armstrong, N. W. Millard, S. D. McPhail, P. Stevenson, M. Pebody, J. Perrett, M. Squires, D. G. Bone (2002), Antarctic krill under sea ice: elevated abundance in a narrow band just south of ice edge, *Science*, *295*, 1890-1892.

Cheon, W. G., S.-K. Lee, A. L. Gordon, Y. Liu, C.-B. Cho and J. Park (2015), Replicating the 1970s' Weddell Polynya using a coupled ocean - sea ice model with reanalysis surface flux fields, *Geophys. Res. Lett*., *42*, 5411-5418, doi:10.1002/2015GL064364.

Clem, K. R., and J. A. Renwick (2015), Austral spring Southern Hemisphere circulation and temperature changes and links to the SPCZ, *J. Clim*., *28*, 7371-7384.

570 Compo, G. P., J. S. Whitaker, P. D. Sardeshmukh, N. Matsui, R. J. Allan, X. Yin, B. E. Gleason
571 R.S. Vose, G. Rutledge, P. Bessemoulin, and S. Brönnimann (2011), The twentieth century
572 reanalysis project, *Q. J. R. Meteorol. Soc*., *137*, 1–28.
573 Danabasoglu, G., S. C. Bates, B. P. Briegleb, S. R. Jayne, M. Jochum, W. G. Large, S. Peacock,
574 and S. G. Yeager (2012), The CCSM4 ocean component, *J. Clim*., *25*, 1361–1389.
575 Dai, A. and K. E. Trenberth (2002), Estimates of freshwater discharge from continents:
576 Latitudinal and seasonal variations, *J. Hydrometeorol*., *3*, 660-687.
577 Dee, D. P., S. M. Uppala, A. J. Simmons, P. Berrisford, P. Poli, S. Kobayashi, U. Andrae, M. A.
578 Balmaseda, G. Balsamo, P. Bauer, and P. Bechtold (2011), The ERA-Interim reanalysis:
579 Configuration and performance of the data assimilation system, *Q. J. R. Meteorol. Soc*., 137,
580 553-597.
581 de Lavergne, C., J. B. Palter, E. D. Galbraith, R. Bernardello, and I. Marinova (2014), Cessation
582 of deep convection in the open Southern Ocean under anthropogenic climate change, *Nat.*
583 *Clim. Change*, *4*, 278–282.
584 Ding, Q., E. J. Steig, D. S. Battisti, and M. Küttel (2011), Winter warming in West Antarctica
585 caused by central tropical Pacific warming, *Nat. Geosci*., *4*, 398-403.
586 Domingues, R., G. Goni, S. Swart, and S. Dong (2014), Wind forced variability of the Antarctic
587 Circumpolar Current south of Africa between 1993 and 2010, *J. Geophys. Res. Oceans*, *119*,
588 1123–1145, doi:10.1002/2013JC008908.
589 Ebert, E. E., and J. A. Curry (1993), An intermediate one-dimensional thermodynamic sea ice
590 model for investigating ice-atmosphere interactions, *J. Geophys. Res*., *98*, 10,085 – 10,109.

591 Enfield, D. B., A. M. Mestas-Nuñez, and P. J. Trimble (2001), The Atlantic multidecadal
592 oscillation and its relation to rainfall and river flows in the continental US., *Geophys. Res.*
593 *Lett*., *28*, 2077-2080.
594 Ferreira, D., J. Marshall, C. M. Bitz, S. Solomon, and A. Plumb (2015), Antarctic Ocean and sea
595 ice response to ozone depletion: A two-time-scale problem, *J. Clim*., *28*, 1206-1226.
596 Gent, P. R., and G. Danabasoglu (2011), Response to increasing Southern Hemisphere winds in
597 CCSM4, *J. Clim.*, *24*, 4992–4998.
598 Ghil, M., and K. C. Mo (1991), Intraseasonal oscillations in the global atmosphere. Part II:
599 Southern Hemisphere. *J. Atmos. Sci*., *48*, 780–790.
600 Gillett, N. P., and D. W. J. Thompson (2003), Simulation of recent Southern Hemisphere climate
601 change, *Science*, *302*, 273-275.
602 Gordon, A. L., and H. W. Taylor (1975), Seasonal change of Antarctic Sea ice cover. *Science*,
603 *187*, 346-347.
604 Gordon, A. L., M. Visbeck, and J. C. Comiso (2007), A possible link between the Weddell
605 Polynya and the Southern Annular Mode, *J. Clim*., *20*, 2558–2571.
606 Gordon, A. L. (2014), Oceanography: Southern Ocean polynya, *Nat. Clim. Change*, *4*, 249-250.
607 Griffies, S. M. (2012), Elements of the modular ocean model (MOM), NOAA/Geophysical Fluid
608 Dynamics Laboratory, Princeton, NJ, 632 pp.
609 Holland, P. R., and R. Kwok (2012), Wind-driven trends in Antarctic sea-ice drift. *Nat. Geosci.*,
610 *5*, 872-875.
611 Hunke, E. C., and W. H. Lipscomb (2008), CICE: The Los Alamos Sea Ice Model,
612 documentation and software, version 4.0. Los Alamos National Laboratory Tech. Rep. LA-
613 CC-06-012, 76pp.

614 Jacobs, S. S., H. Hellmer, C. Doake, and R. Frolich (1992), Melting of ice shelves and the mass
615 balance of Antarctica, *J. Glaciol*., *38*, 375–387.
616 Ji, X., J. D. Neelin, S.-K. Lee, and C. R. Mechoso (2014), Interhemispheric teleconnections from
617 tropical heat sources in intermediate and simple models, *J. Clim.*, *27*, 684-697.
618 Kirtman, B. P., C. M. Bitz, F. Bryan, W. Collins, J. Dennis, N. Hearn, J. L. Kinter III, R. Loft, C.
619 Rousset, L. Siqueira, and C. Stan (2012), Impact of ocean model resolution on CCSM
620 climate simulations, *Clim. Dyn*., *39*, 1303 - 1328.
621 Kwok, R., and J. C. Comiso (2002), Southern Ocean climate and sea ice anomalies associated
622 with the Southern Oscillation, *J. Clim.*, *15*, 487-501.
623 Landrum, L., M. M. Holland, D. P. Schneider, E. Hunke (2012), Antarctic sea ice climatology,
624 variability, and late twentieth-century change in CCSM4, *J. Clim.*, *25*, 4817-4838.
625 Large, W. G., and S. G. Yeager (2009), The global climatology of an interannually varying air–
626 sea flux data set, *Clim. Dyn.*, *33*, 341–364.
627 Lau, M. K., P. J. Sheu, and I. S. Kang (1994), Multiscale low-frequency circulation modes in the
628 global atmosphere, *J. Atmos. Sci*., *51*, 2753–2750.
629 Lee, S. and S. B. Feldstein (2013), Detecting ozone-and greenhouse gas–driven wind trends with
630 observational data, *Science*, *339*, 563-567.
631 Lee, S.-K., D. B. Enfield, and C. Wang (2007), What drives seasonal onset and decay of the
632 Western Hemisphere warm pool?, *J. Clim*, *20*, 2133-2146.
633 Lee, S.-K., C. R. Mechoso, C. Wang, and J. D. Neelin (2013), Interhemispheric influence of the
634 northern summer monsoons on the southern subtropical anticyclones, *J. Clim.*, *26*, 10193-
635 10204.

636 Lee, S.-K., W. Park, E. van Sebille, M. O. Baringer, C. Wang, D. B. Enfield, S. Yeager and B. P.
637 Kirtman (2011), What caused the significant increase in Atlantic ocean heat content since the
638 mid-20th century?, *Geophys. Res. Lett*., *38*, L17607, doi:10.1029/2011GL048856
639 Lee, S.-K., W. Park, M. O. Baringer, A. L. Gordon, B. Huber and Y. Liu (2015), Pacific origin
640 of the abrupt increase in Indian Ocean heat content during the warming hiatus, *Nat. Geosci.*,
641 *8*, 445-449, doi:10.1038/ngeo2438.
642 Legler, D. M., H. J. Freeland, R. Lumpkin, G. Ball, M. J. McPhaden, S. North, R. Crowley, G. J.
643 Goni, U. Send and M. A. Merrifield (2015), The current status of the real-time in situ global
644 ocean observing system for operational oceanography, *J. Oper. Oceanogr*, *8*, sup2, s189-
645 s200.
646 Li, X., D. M. Holland, E. P. Gerber, and C. Yoo (2014), Impacts of the north and tropical
647 Atlantic Ocean on the Antarctic Peninsula and sea ice, *Nature, 505*, 538-542.
648 Limpasuvan, V., and D. L. Hartmann (1999), Eddies and the annular modes of climate
649 variability, *Geophys. Res. Lett*., *26*, 3133-3136, doi:10.1029/1999GL010478.
650 Liu, J., J. A. Curry, and D. G. Martinson (2004), Interpretation of recent Antarctic sea ice
651 variability, *Geophys. Res. Lett*., *31*, L02205, doi:10.1029/2003GL018732.
652 Liu, Y., S.-K. Lee, D. B. Enfield, B. A. Muhling, J. T. Lamkin, F. Muller-Karger and M. A.
653 Roffer (2015), Potential impact of climate change on the Intra-Americas Seas: Part-1. A
654 dynamic downscaling of the CMIP5 model projections. *J. Marine Syst*., *148*, 56-69,
655 doi:10.1016/j.jmarsys.2015.01.007.
656 Lopez, H., S. Dong, S.-K. Lee, and E. Campos (2016), Remote influence of Interdecadal Pacific
657 Oscillation on the South Atlantic meridional overturning circulation variability, *Geophys.*
658 *Res. Lett*., *43*, 8250–8258, doi:10.1002/2016GL069067.

659 Matear, R. J., T. J. O'Kane, J. S. Risbey, and M. Chamberlain (2015), Sources of heterogeneous
660 variability and trends in Antarctic sea-ice. *Nat. Commun.*, *6*, 8656.
661 Meehl, G. A., J. M. Arblaster, J. Y. Fasullo, A.Hu, and K. E. Trenberth (2011), Model-based
662 evidence of deep ocean heat uptake during surface temperature hiatus periods, *Nat. Clim.*
663 *Change*, *1*, 360 – 364.
664 Meehl, G. A., J. M. Arblaster, C. M. Bitz, C. T. Chung, and H. Teng (2016), Antarctic sea-ice
665 expansion between 2000 and 2014 driven by tropical Pacific decadal climate variability, *Nat.*
666 *Geosci*., doi:10.1038/ngeo2751.
667 Meyer, B., A. Atkinson, B. Blume, and U. V. Bathmann (2002), Feeding and energy budgets of
668 Antarctic krill Euphausia superba at the onset of winter–I–Furcilia III larvae, *Limnol.*
669 *Oceanogr*., *47*, 943–952.
670 Mo, K. C., and R. W. Higgins (1998), The Pacific-South American modes and tropical
671 convection during the Southern Hemisphere winter, *Mon. Weather Rev.*, *126*, 1581-1596.
672 Parkinson, C. L., and D. J. Cavalieri (2012), Antarctic sea ice variability and trends, 1979–2010,
673 *Cryosphere*, *6*, 871-880, doi:10.5194/tc-6-871-2012, 2012.
674 Piñones, A. and A. V. Fedorov (2016), Projected changes of Antarctic krill habitat by the end of
675 the 21st century, *Geophys. Res. Lett*., *43*, doi:10.1002/2016GL069656.
676 Purich, A., M. H. England, W. Cai, Y. Chikamoto, A. Timmermann, J. C. Fyfe, L. Frankcombe,
677 G. A. Meehl, and J. M. Arblaster (2016), Tropical Pacific SST drivers of recent Antarctic sea
678 ice trends, *J. Clim.*, doi:10.1175/JCLI-D-16-0440.1, in press.
679 Rayner, N. A., D. E. Parker, E. B. Horton, C. K. Folland, L. V. Alexander, D. P. Rowell, E. C.
680 Kent, and A. Kaplan (2003), Global analyses of sea surface temperature, sea ice, and night

marine air temperature since the late nineteenth century, *J. Geophys. Res.*, *108*, 4407, doi:10.1029/2002JD002670, D14.

Renwick, J. A. (2002), Southern Hemisphere circulation and relations with sea ice and sea surface temperature, *J. Clim.*, *15*, 3058-3068.

Rienecker, M. M. et al. (2011), MERRA: NASA's Modern-Era Retrospective analysis for Research and Applications, *J. Clim.*, *24*, 3624-3648, doi:10.1175/JCLI-D-11-00015.1.

Rignot, E., S. Jacobs, J. Mouginot, and B. Scheuchl (2013), Ice-shelf melting around Antarctica, *Science*, *341*, 266-270.

Rintoul, S. R., M. Sparrow, M. P. Meredith, V. Wadley, K. Speer, E. Hofmann, C. P. Summerhayes, E. Urban, R. Bellerby, S. Ackley, and K. Alverson (2012), The Southern Ocean observing system: initial science and implementation strategy, Cambridge, UK: Scientific Committee on Antarctic Research, 74 pp.

Russell, J. R., J. L. Sarmiento, H. Cullen, R. Hotinski, K. Johnson, S. Riser, and L. Talley (2014), The Southern Ocean Carbon and Climate Observations and Modeling Program (SOCCOM), *Ocean Carbon and Biogeochemistry Newsletter*, *7*, 1-5.

Rysgaard, S., J. Bendtsen, B. Delille, G. S. Dieckmann, R. N. Glud, H. Kennedy, J. Mortensen, S. Papadimitriou, D. N. Thomas, and J.-L. Tison (2011), Sea ice contribution to the air-sea CO_2 exchange in the Arctic and Southern Oceans, *Tellus B*, *63*, 823-830.

Shindell, D. T., and G. A. Schmidt (2004), Southern Hemisphere climate response to ozone changes and greenhouse gas increases, *Geophys. Res. Lett.*, *31*, L18209, doi:10.1029/2004GL020724.

Simpkins, G. R., S. McGregor, A. S. Taschetto, L. M. Ciasto, M. H. England (2014), Tropical connections to climatic change in the extratropical Southern Hemisphere: The role of Atlantic SST trends, *J. Clim.*, *27*, 4923-4936.

Son, S.-W., L. M. Polvani, D. W. Waugh, H. Akiyoshi, R. R. Garcia, D. Kinnison, S. Pawson, E. Rozanov, T. G. Shepherd, and K. Shibata (2008), The impact of stratospheric ozone recovery on the Southern Hemisphere westerly jet, *Science*, *320*, 1486–1489.

Stammerjohn, S. E., D. G. Martinson, R. C. Smith, X. Yuan, D. and Rind (2008), Trends in Antarctic annual sea ice retreat and advance and their relation to El Niño–Southern Oscillation and Southern Annular Mode variability, *J. Geophys. Res.*, *113*, C03S90, doi:10.1029/2007JC004269.

Steele, M., R. Morley, and W. Ermold (2001), A global ocean hydrography with a high-quality Arctic Ocean, *J. Clim.*, *14*, 2079–2087.

Stroeve, J. C., V. Kattsov, A. Barrett, M. Serreze, T. Pavlova, M. Holland, and W. N. Meier (2012), Trends in Arctic sea ice extent from CMIP5, CMIP3 and observations, *Geophys. Res. Lett.*, *39*, L16502, doi:10.1029/2012GL052676.

Takahashi, T., S. C. Sutherland, R., Wanninkhof, C. Sweeney, R. A. Feely, D. W. Chipman, B. Hales, G. Friederich, F. Chavez, C. Sabine, A. Watson, D. C. E. Bakker, U. Schuster, N. Metzl, H. Y. Inoue, M. Ishii, T. Midorikawa, Y. Nojiri, A. Koertzinger, T. Steinhoff, M. Hoppema et al. (2009), Climatological mean and decadal change in surface ocean pCO_2, and net sea-air CO_2 flux over the global oceans, *Deep-Sea Res. II*, *56*, 554–577, doi:10.1016/j.dsr2.2008.12.009.

Talley L. D., G. L. Pickard, W. J. Emery, J. H. Swift (2011), Descriptive physical oceanography: An introduction (Sixth Edition), Elsevier, Boston, 560 pp.

Thompson, D. W. J., and S. Solomon (2002), Interpretation of recent Southern Hemisphere climate change, *Science*, 296, 895-899.

Turner, J., and J. Overland (2009), Contrasting climate change in the two polar regions, *Polar Res.*, *28*, 146–164.

Walsh, J. E. (1983), The role of sea ice in climatic variability: Theories and evidence, *Atmos.-Ocean*, *21*, 229 - 242.

Wang, C., S.-K. Lee, and C. R. Mechoso (2010), Inter-hemispheric influence of the Atlantic warm pool on the southeastern Pacific, *J. Clim.*, *23*, 404-418.

Wanninkhof, R., G.-H. Park, T. Takahashi, C. Sweeney, R. Feely, Y. Nojiri, N. Gruber, S. C. Doney, G. A. McKinley, A. Lenton, C. Le Quéré, C. Heinze, J. Schwinger, H. Graven and S. Khatiwala (2013), Global ocean carbon uptake: magnitude, variability and trends, *Biogeosciences*, *10*, 1983-2000.

Wu, Y., X. Zhai, X, and Z. Wang (2016), Impact of synoptic atmospheric forcing on the mean ocean circulation, *J. Clim*., *29*, 5709 - 5724.

Yuan, X. (2004), ENSO-related impacts on Antarctic sea ice: a synthesis of phenomenon and mechanisms, *Antarct. Sci*., *16*, 415-25.

Yuan, X., and C. Li (2008), Climate modes in southern high latitudes and their impacts on Antarctic sea ice, *J. Geophys. Res.*, *113*, C06S91, doi:10.1029/2006JC004067.

Zhang, J. (2007), Increasing Antarctic sea ice under warming atmospheric and oceanic conditions, *J. Clim*., *20*, 2515 - 2529.

Zhang, L., T. L. Delworth, and F. Zeng (2016), The impact of multidecadal Atlantic meridional overturning circulation variations on the Southern Ocean, *Clim. Dyn*., doi:10.1007/s00382-016-3190-8.

748

749 **Figure 1.** Linear trends of Antarctic sea-ice concentration during (a,c) the warm (December -
750 May) and (b,d) cold (June - November) seasons, obtained from (a,b) the Hadley Center sea ice
751 and sea surface temperature data sets over the period of 1979 - 2014 and (c,d) the historical
752 simulation over the period of 1985 - 2014. The first six years (1979 - 1984) of the model results
753 were excluded to prevent any potential model drift in the beginning of the historical simulation
754 from affecting the modeled sea-ice trend. The units are % in 35 years.

755

756 **Figure 2.** The oceans and regional seas around Antarctica. The East Pacific sector (150°W -
757 80°W), indicated by the light red lines, includes part of the Bellingshausen Sea west of the
758 Antarctic peninsula, the Amundsen Sea, and part of the Ross Sea east of 150°W. The Atlantic
759 sector (60°W - 0°), indicated by the light blue lines, includes the Weddell Sea.

760

761 **Figure 3.** Linear trends of Antarctic sea-ice concentration averaged in (a,b) the East Pacific
762 (150°W - 80°W) and (c,d) Atlantic (60°W - 0°) sectors for each calendar month, obtained from
763 (a,c) the historical simulation over the period of 1984 - 2014 and (b,d) the Hadley Center sea ice
764 and sea surface temperature data sets over the period of 1979 - 2014. The two green lines in each
765 panel represent the 5% and 90% climatological sea-ice concentration boundaries. The color scale
766 units are % in 35 years.

767

768 **Figure 4.** Linear trends of (a,b) Antarctic sea-ice concentration and (c,d) ocean temperatures
769 averaged in the East Pacific sector (150°W - 80°W) for (a,c) the warm and (b,d) cold seasons
770 over the period of 1985 - 2014, obtained from the historical simulation. Observed linear trends of

771 Antarctic sea-ice concentration over the period of 1979 - 2014 averaged in the East Pacific sector
772 are also shown in (a,b). The black lines in (c,d) indicate the climatological temperatures. The
773 units are % in 35 years for sea-ice concentration and °C in 35 years for ocean temperature.
774
775 **Figure 5.** Linear trends of (a) vertical velocity at 100 m (shades) and wind stress curl (contours),
776 and (b) meridional velocity averaged in the upper 100 m (shades) and zonal wind stress
777 (contours) over the period of 1985 - 2014 averaged in the East Pacific sector (150°W - 80°W)
778 for each of calendar month, obtained from the historical simulation. These fields are not shown
779 for the interior of the climatological ice pack (i.e., above 90% sea-ice concentration). (c)
780 Anomalies of advective heat flux (ΔQ_{ADV}), storage rate (ΔQ_{STR}), and residual heat flux (ΔQ_{RES})
781 in the upper 100 m, and net air-sea surface heat flux (ΔQ_{SHF}) averaged in (left panel) the 75°S -
782 70°S and (right panel) 68°S - 60°S latitude bands over the East Pacific sector. These heat flux
783 anomalies are derived from the historical simulation (the averages for the 1985-2014 periods)
784 relative to the reference simulation (the averages for 600 years). The units are 10^{-2} m s^{-1} in 35
785 years for meridional velocity, 10^{-4} m s^{-1} in 35 years for vertical velocity and 10^{-6} N m^{-3} in 35
786 years for wind stress curl, % in 35 years for sea-ice fraction, and W m^{-2} for heat fluxes.
787
788 **Figure 6.** Linear trends of sea level pressure (shades) derived from MERRA and surface wind
789 stress vectors (arrows) derived from the historical simulation over the period of 1985 - 2014
790 during (a) the warm and (b) cold seasons. The units are hPa in 35 years for sea level pressure,
791 and 10^{-1} Nm^2 in 35 years for wind stress vectors.
792

Figure 7. Linear trend (green colors) and climatology (black colors) of the surface zonal wind stress averaged in (a) the East Pacific (150°W - 80°W) and (b) Atlantic (60°W - 0°) sectors, derived from the historical simulation over the period of 1985 - 2014. The units are 10^{-1} N m^2 in 35 years.

Figure 8. Linear trends of (a,b) Antarctic sea-ice concentration, (c,d) ocean temperatures, and (e,f) zonal velocity averaged over the Atlantic sector (60°W - 0°) for (a,c,e) the warm and (b,d,e) cold seasons over the period of 1985 - 2014, obtained from the historical simulation. Observed linear trends of Antarctic sea-ice concentration over the period of 1979 – 2014 averaged over the Atlantic sector are also shown in (a,b). The black lines in (c,d) and (e,f) indicate the climatological temperatures and zonal velocity, respectively. The units are % in 35 years for sea-ice concentration, °C in 35 years for ocean temperature and cm s^{-1} in 35 years for zonal velocity.

Figure 9. As in Figure 5, but for the Atlantic sector (60°W - 0°) and (c) averaged over (left panel) the 80°S - 68°S and (right panel) 66°S - 54°S latitude bands over the Atlantic sector.

Figure 10. Upper 3000 m ocean heat budget in the Atlantic sector (60°W - 0°). (a) Advective heat flux (Q_{ADV}), storage rate (Q_{STR}), and residual heat flux (Q_{RES}) in the upper 3000 m, and net air-sea surface heat flux (Q_{SHF}) averaged in the Atlantic sector in (left panels) the 80°S - 66°S and (right panels) 62°S - 52°S latitude bands, derived from the reference simulation (the averages for 600 years). (b) The changes (or anomalies) in the four heat budget terms (ΔQ_{ADV}, ΔQ_{STR}, ΔQ_{RES}, and ΔQ_{SHF}) during the 1985-2014 periods, derived from the historical simulation

(the averages for the 1985-2014 periods) relative to the reference simulation (the averages for 600 years). The units are W m^{-2}.

Figure 11. Leading Empirical Orthogonal Function (EOF) modes of detrended Antarctic sea-ice concentration variability during (a,c) the warm and (b,d) cold seasons, obtained from (a,b) the Hadley Center sea ice and sea surface temperature data sets over the period of 1979 - 2014 and (c,d) the historical simulation over the period of 1985 - 2014. The normalized principal components (PCs) of the leading modes are shown in (e,f). The percentage variance explained by each of the leading modes, and the correlations between the PCs derived from the observations and the historical simulation are indicated in (e,f). The units in (a-d) are % per two units of the normalized PCs.

Figure 12. Sketch of the physical mechanisms linking the wind-driven ocean dynamics and the Antarctic sea-ice trends in (a) the East Pacific (150°W - 80°W) and (b) Atlantic (60°W - 0°) sectors. In the East Pacific sector, the strengthening SH westerlies enhanced Ekman upwelling of the warm upper CDW and increased the northward Ekman transport of cold Antarctic surface water, thus contributing to the expansion of sea-ice in the cold seasons and to the retreat in the warm seasons. In the Atlantic, the poleward shifting SH westerlies strengthened the northern branch of the Weddell Gyre. The strengthened the Weddell Gyre acted as a barrier against the poleward ocean heat transport, and thus produced anomalous heat divergence within the Weddell Gyre and anomalous heat convergence north of the gyre. Hence, the meridional thermal gradient increased across the northern branch of the Weddell Gyre, as also constrained by the thermal wind balance, cooling the water column within the Weddell Gyre and warming the water column

838 north of the gyre, thus contributing to the expansion of sea-ice in the warm seasons, and the
839 retreat in the cold seasons.

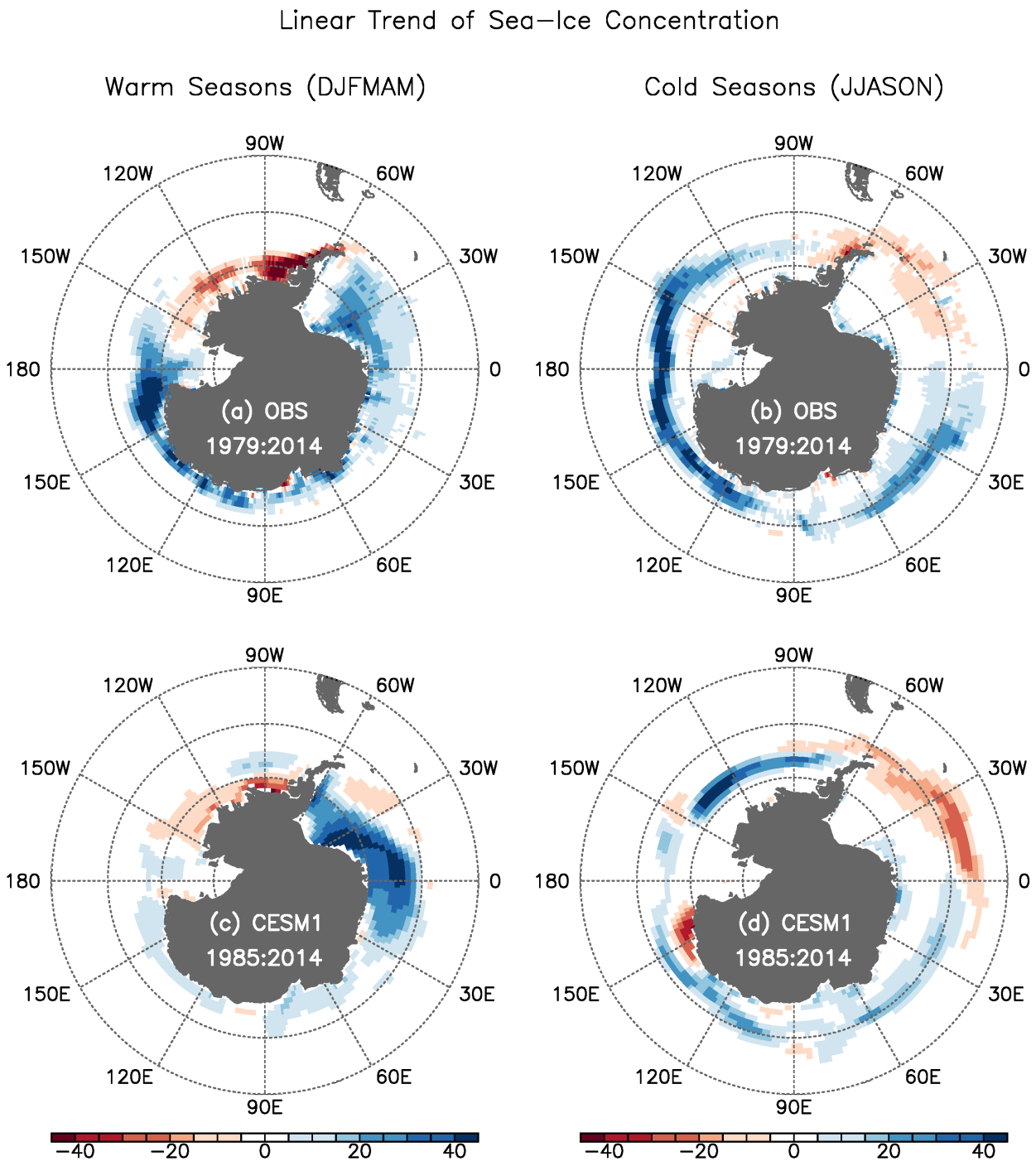

Figure 1. Linear trends of Antarctic sea-ice concentration during (a,c) the warm (December - May) and (b,d) cold (June - November) seasons, obtained from (a,b) the Hadley Center sea ice and sea surface temperature data sets over the period of 1979 - 2014 and (c,d) the historical simulation over the period of 1985 - 2014. The first six years (1979 - 1984) of the model results were excluded to prevent any potential model drift in the beginning of the historical simulation from affecting the modeled sea-ice trend. The units are % in 35 years.

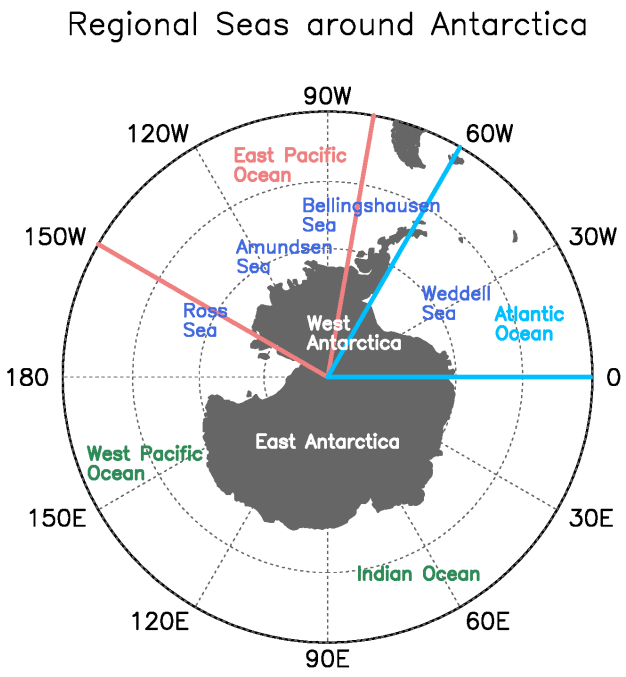

Figure 2. The oceans and regional seas around Antarctica. The East Pacific sector (150°W - 80°W), indicated by the light red lines, includes part of the Bellingshausen Sea west of the Antarctic peninsula, the Amundsen Sea, and part of the Ross Sea east of 150°W. The Atlantic sector (60°W - 0°), indicated by the light blue lines, includes the Weddell Sea**.**

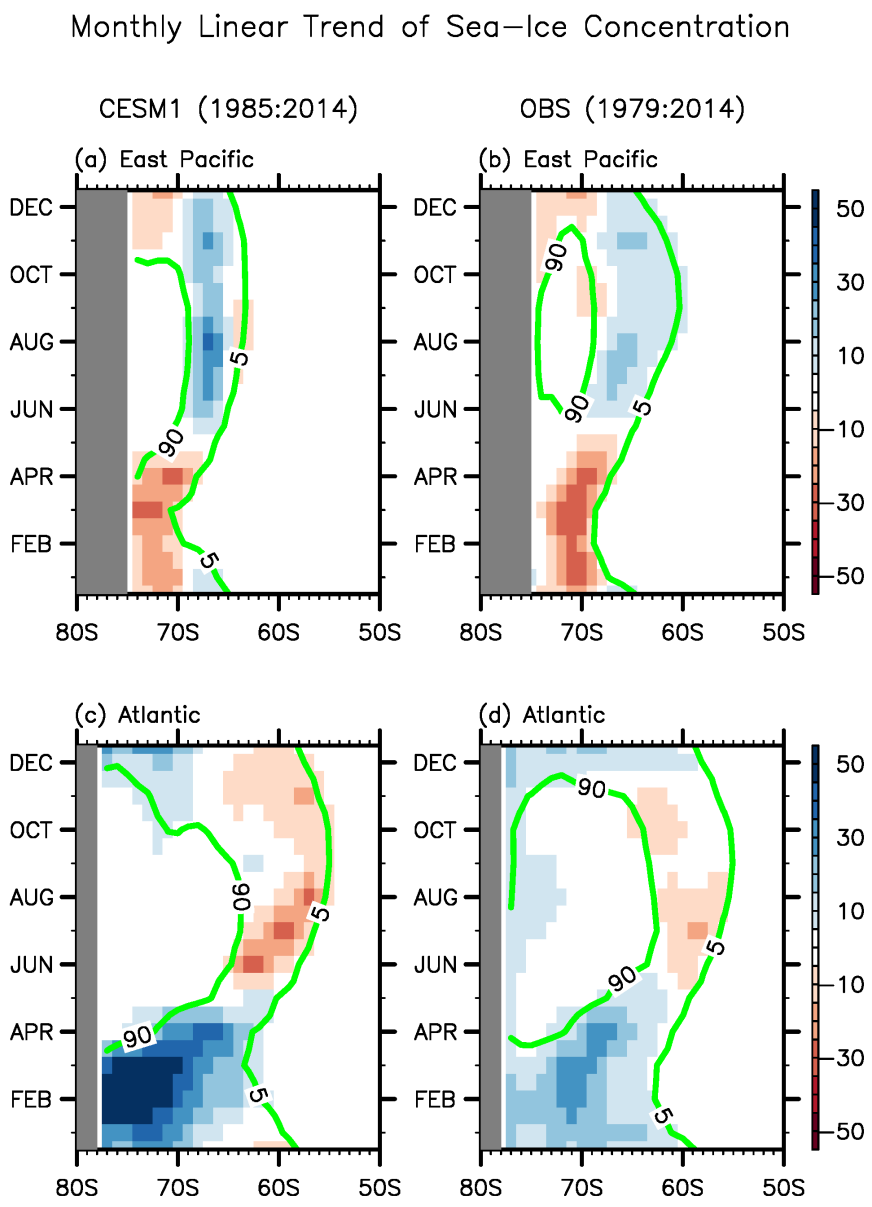

Figure 3. Linear trends of Antarctic sea-ice concentration averaged in (a,b) the East Pacific (150°W - 80°W) and (c,d) Atlantic (60°W - 0°) sectors for each calendar month, obtained from (a,c) the historical simulation over the period of 1984 - 2014 and (b,d) the Hadley Center sea ice and sea surface temperature data sets over the period of 1979 - 2014. The two green lines in each panel represent the 5% and 90% climatological sea-ice concentration boundaries. The color scale units are % in 35 years.

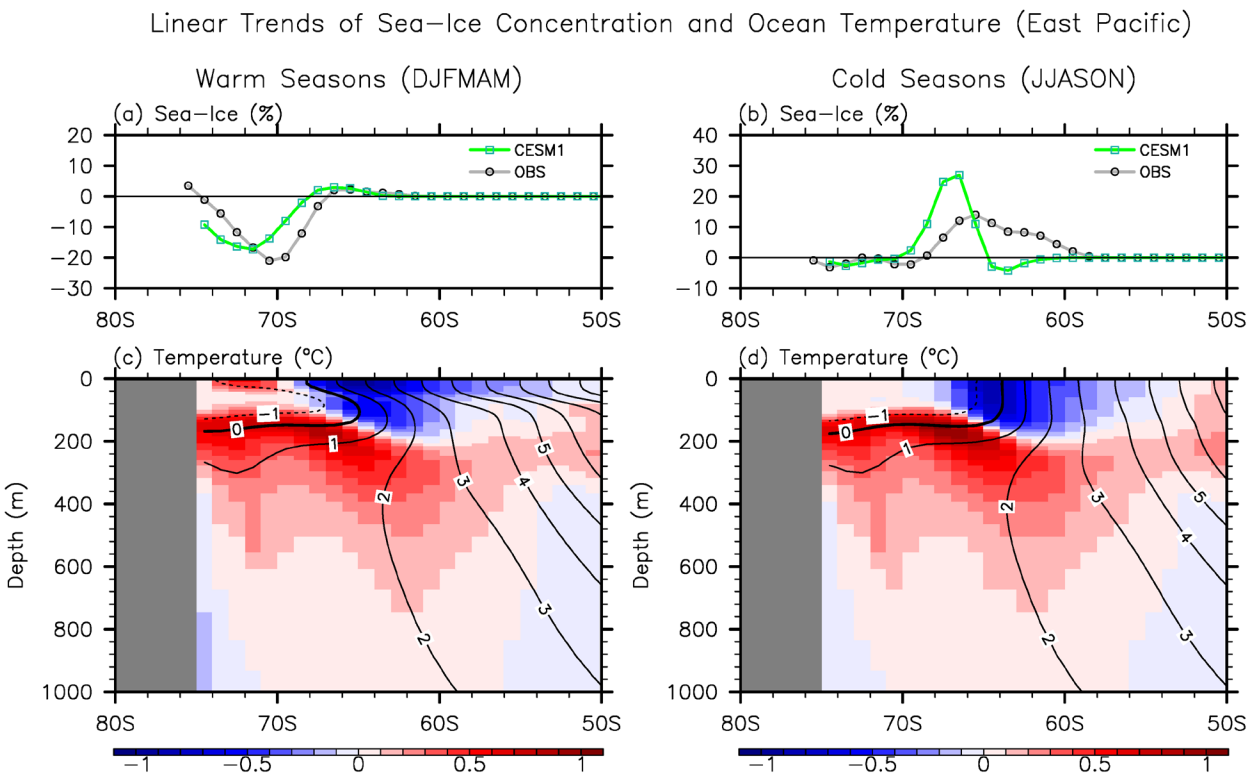

Figure 4. Linear trends of (a,b) Antarctic sea-ice concentration and (c,d) ocean temperatures averaged in the East Pacific sector (150°W - 80°W) for (a,c) the warm and (b,d) cold seasons over the period of 1985 - 2014, obtained from the historical simulation. Observed linear trends of Antarctic sea-ice concentration over the period of 1979 - 2014 averaged in the East Pacific sector are also shown in (a,b). The black lines in (c,d) indicate the climatological temperatures. The units are % in 35 years for sea-ice concentration and °C in 35 years for ocean temperature.

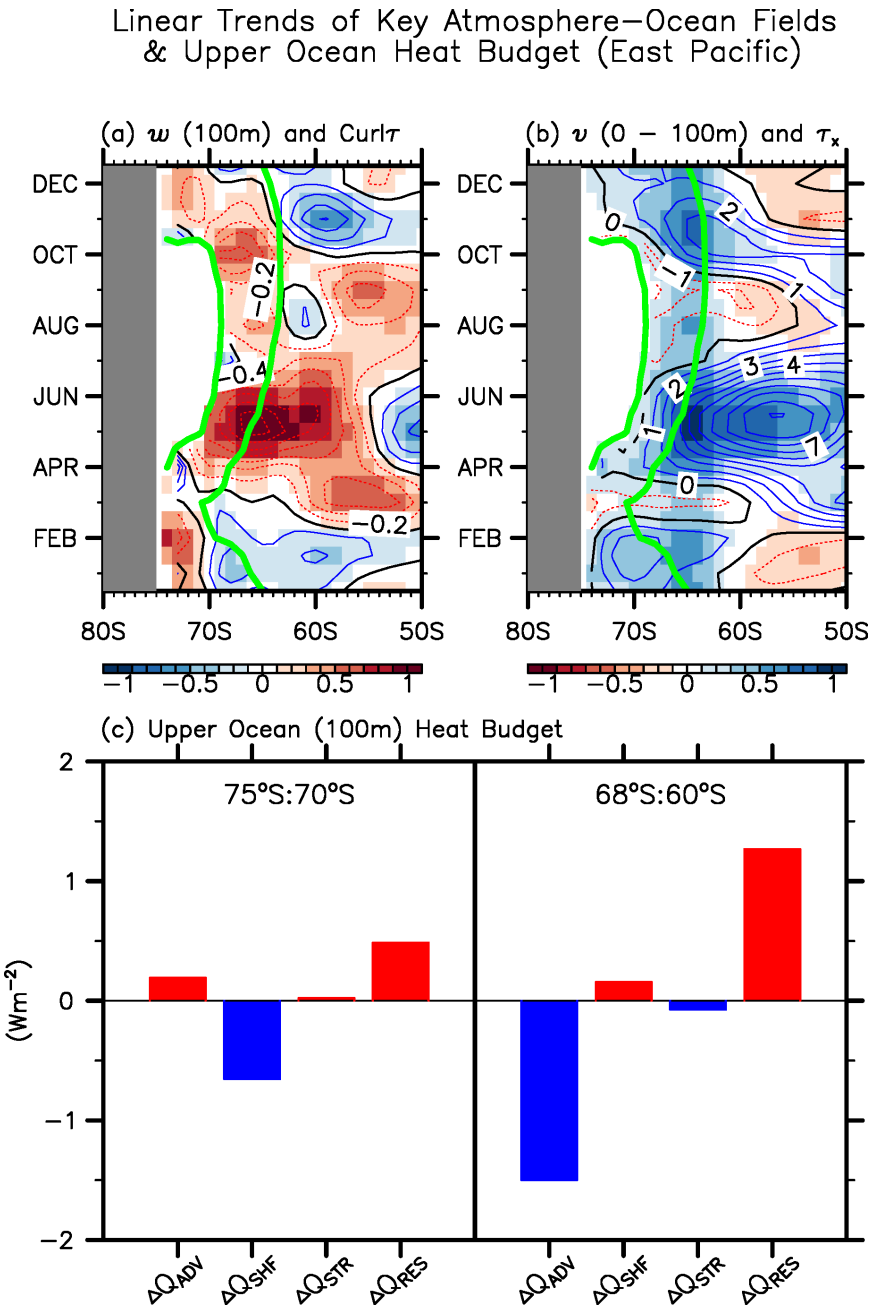

Figure 5. Linear trends of (a) vertical velocity at 100 m (shades) and wind stress curl (contours), and (b) meridional velocity averaged in the upper 100 m (shades) and zonal wind stress (contours) over the period of 1985 - 2014 averaged in the East Pacific sector (150°W - 80°W) for each of calendar month, obtained from the historical simulation. These fields are not shown for the interior of the climatological ice pack (i.e., above 90% sea-ice concentration). (c) Anomalies of advective heat flux (ΔQ_{ADV}), storage rate (ΔQ_{STR}), and residual heat flux (ΔQ_{RES}) in the upper 100 m, and net air-sea surface heat flux (ΔQ_{SHF}) averaged in (left panel) the 75°S - 70°S and (right panel) 68°S - 60°S latitude bands over the East Pacific sector. These heat flux anomalies are derived from the historical simulation (the averages for the 1985-2014 periods) relative to the

reference simulation (the averages for 600 years). The units are 10^{-2} m s^{-1} in 35 years for meridional velocity, 10^{-4} m s^{-1} in 35 years for vertical velocity and 10^{-6} N m^{-3} in 35 years for wind stress curl, % in 35 years for sea-ice fraction, and W m^{-2} for heat fluxes.

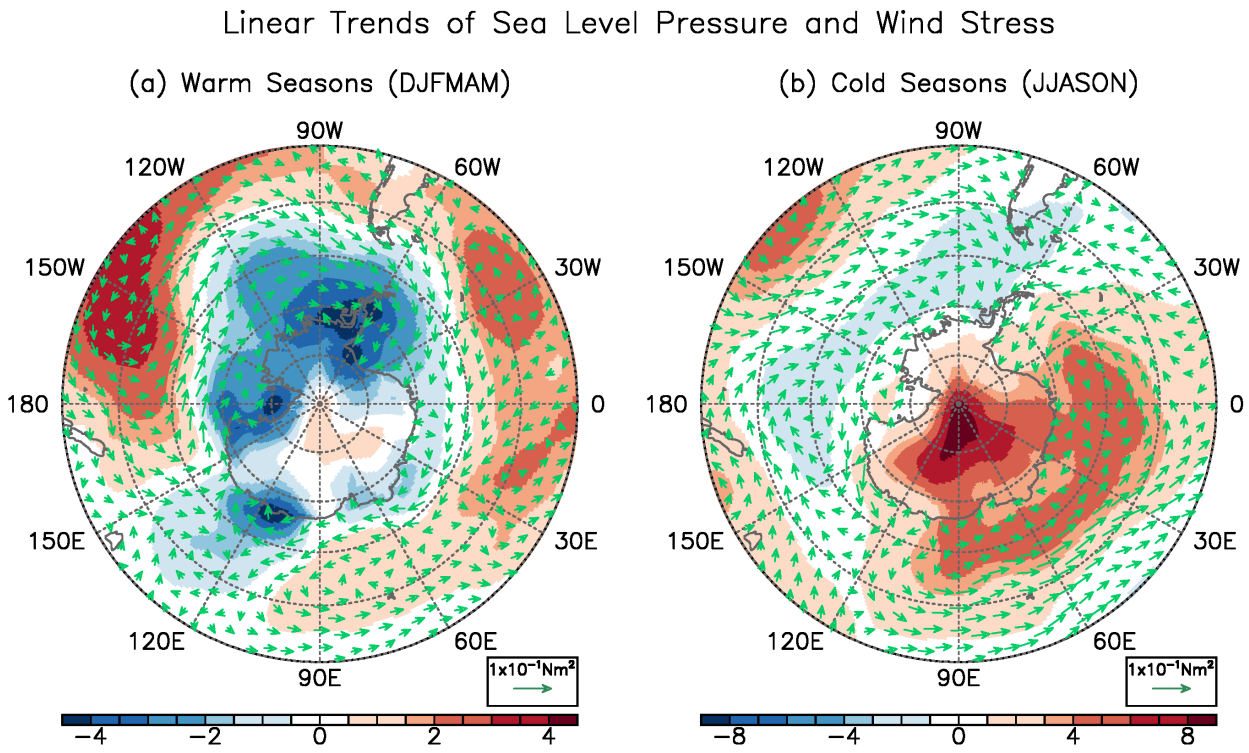

Figure 6. Linear trends of sea level pressure (shades) derived from MERRA and surface wind stress vectors (arrows) derived from the historical simulation over the period of 1985 - 2014 during (a) the warm and (b) cold seasons. The units are hPa in 35 years for sea level pressure, and 10^{-1} N m^2 in 35 years for wind stress vectors.

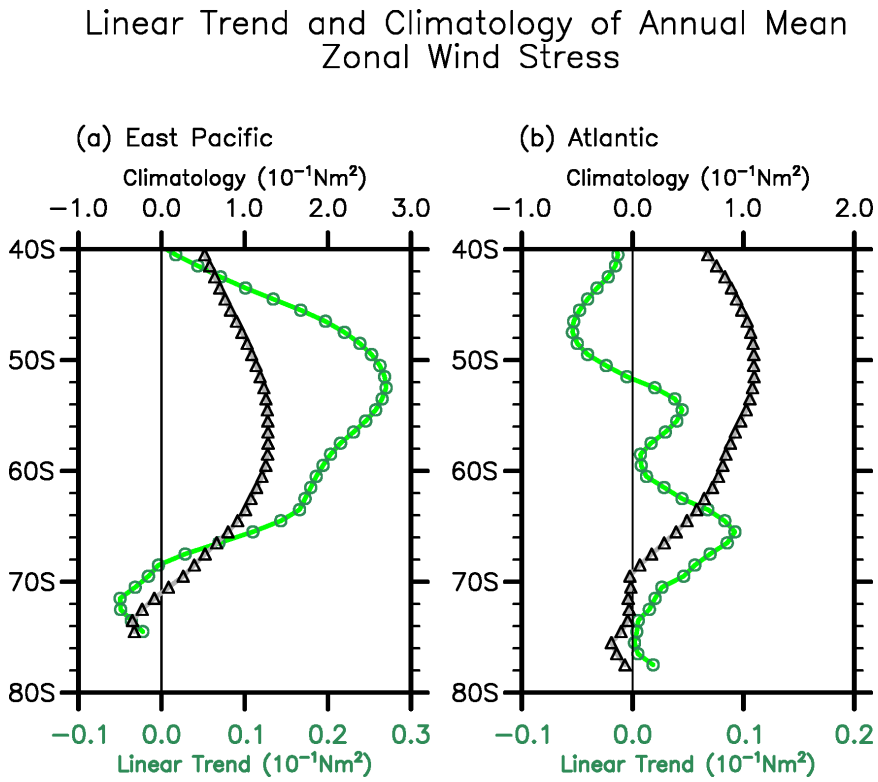

Figure 7. Linear trend (green colors) and climatology (black colors) of the surface zonal wind stress averaged in (a) the East Pacific (150°W - 80°W) and (b) Atlantic (60°W - 0°) sectors, derived from the historical simulation over the period of 1985 - 2014. The units are 10^{-1} N m^2 in 35 years.

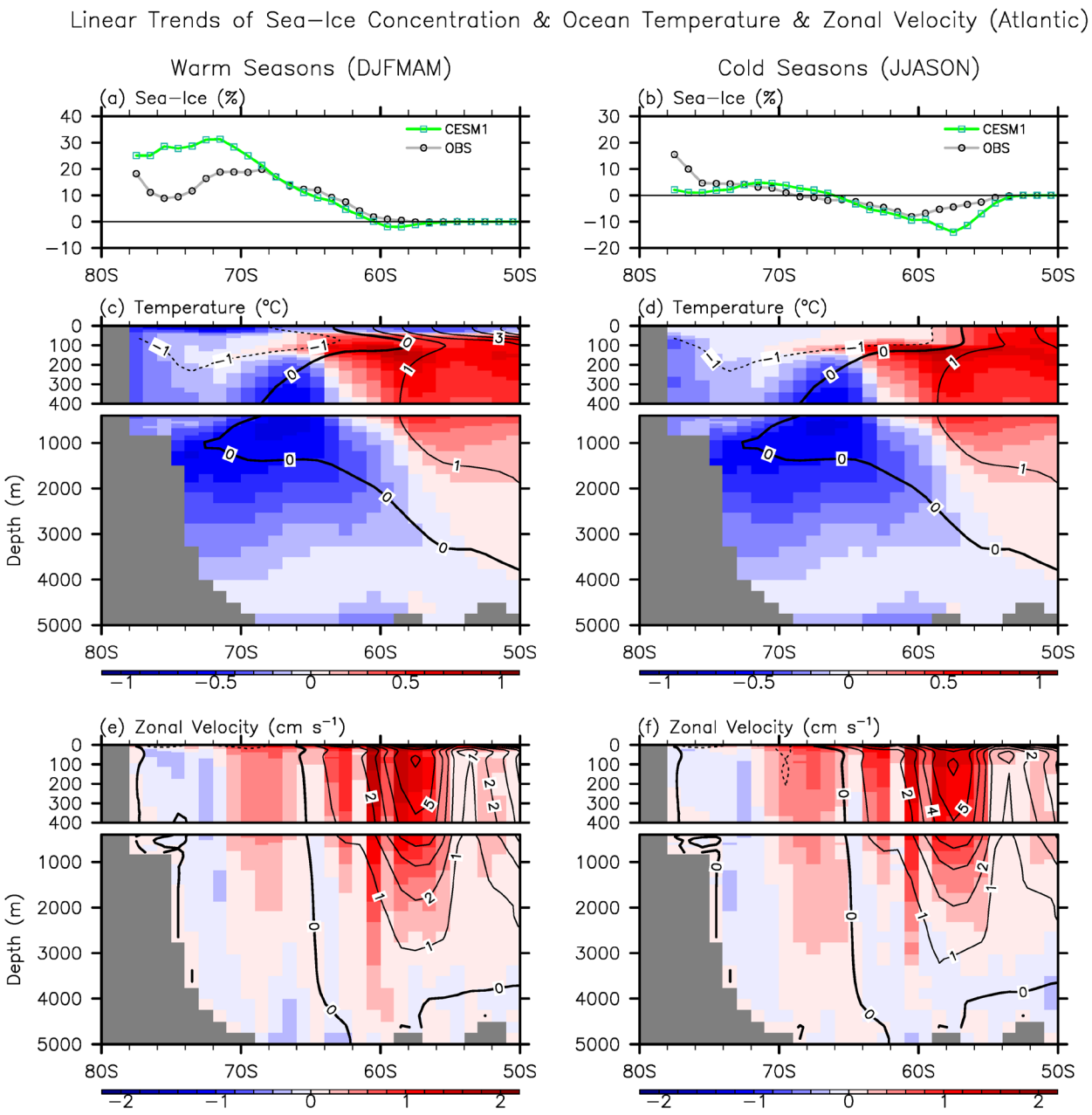

Figure 8. Linear trends of (a,b) Antarctic sea-ice fraction, (c,d) ocean temperatures, and (e,f) zonal velocity averaged in the Atlantic sector (60°W - 0°) for (a,c,e) the warm and (b,d,e) cold seasons over the period of 1985 - 2014, obtained from the historical simulation. Observed linear trends of Antarctic sea-ice fraction over the period of 1979 – 2014 averaged in the Atlantic sector are also shown in (a,b). The black lines in (c,d) and (e,f) indicate the climatological temperatures and zonal velocity, respectively. The units are % in 35 years for sea-ice fraction, °C in 35 years for ocean temperature and cm s^{-1} in 35 years for zonal velocity.

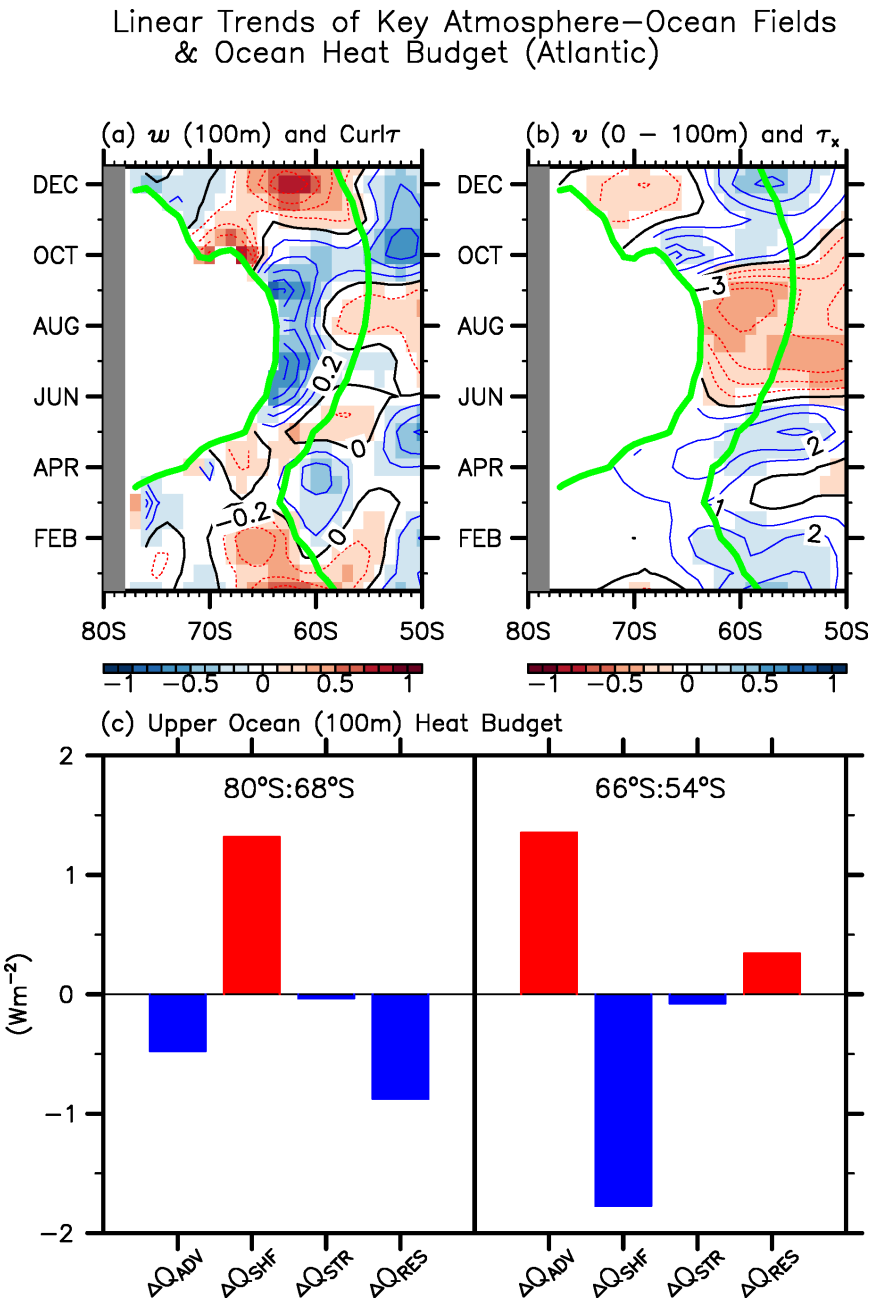

Figure 9. As in Figure 5, but for the Atlantic sector (60°W - 0°) and (c) averaged in (left panel) the 80°S - 68°S and (right panel) 66°S - 54°S latitude bands over the Atlantic sector.

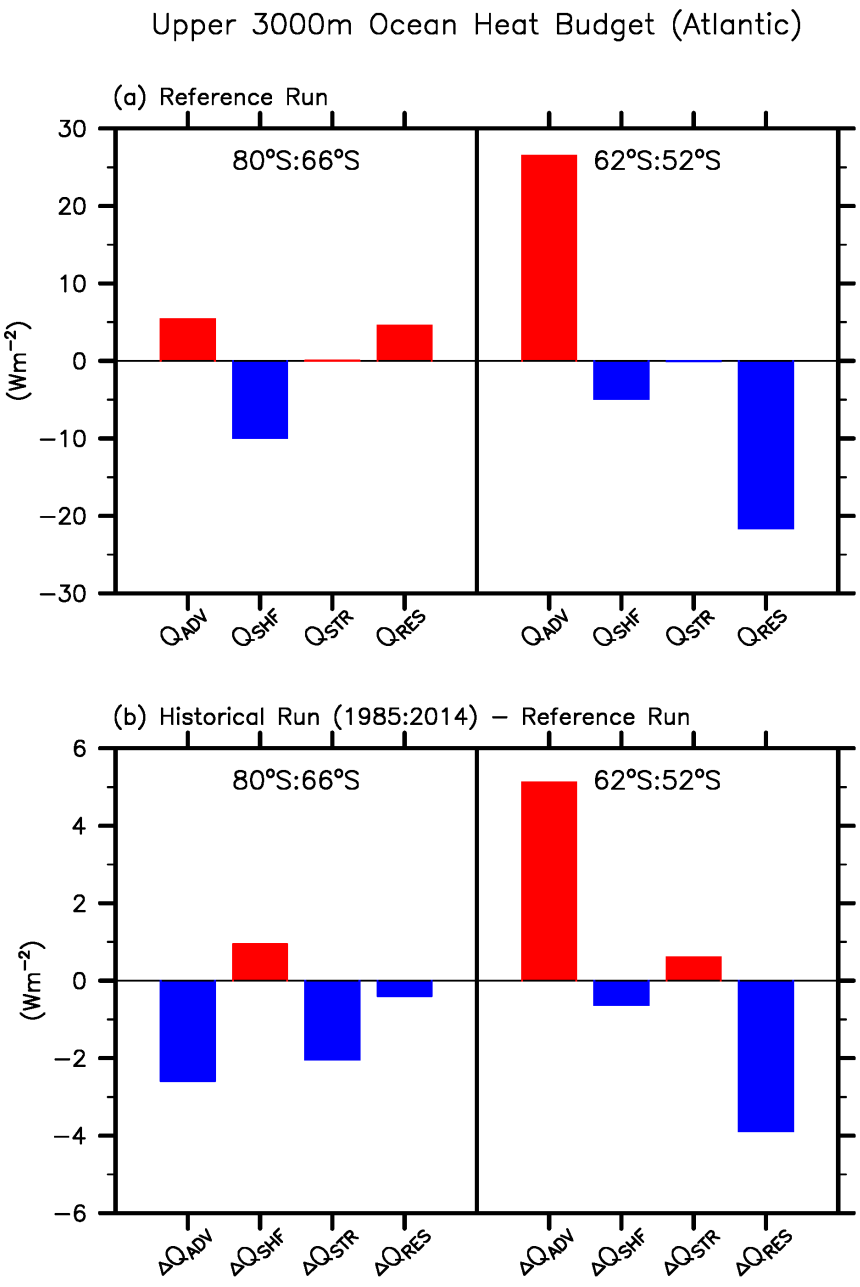

Figure 10. Upper 3000 m ocean heat budget in the Atlantic sector (60°W - 0°). (a) Advective heat flux (Q_{ADV}), storage rate (Q_{STR}), and residual heat flux (Q_{RES}) in the upper 3000 m, and net air-sea surface heat flux (Q_{SHF}) averaged in the Atlantic sector in (left panels) the 80°S - 66°S and (right panels) 62°S - 52°S latitude bands, derived from the reference simulation (the averages for 600 years). (b) The changes (or anomalies) in the four heat budget terms (ΔQ_{ADV}, ΔQ_{STR}, ΔQ_{RES}, and ΔQ_{SHF}) during the 1985-2014 periods, derived from the historical simulation (the averages for the 1985-2014 periods) relative to the reference simulation (the averages for 600 years). The units are W m^{-2}.

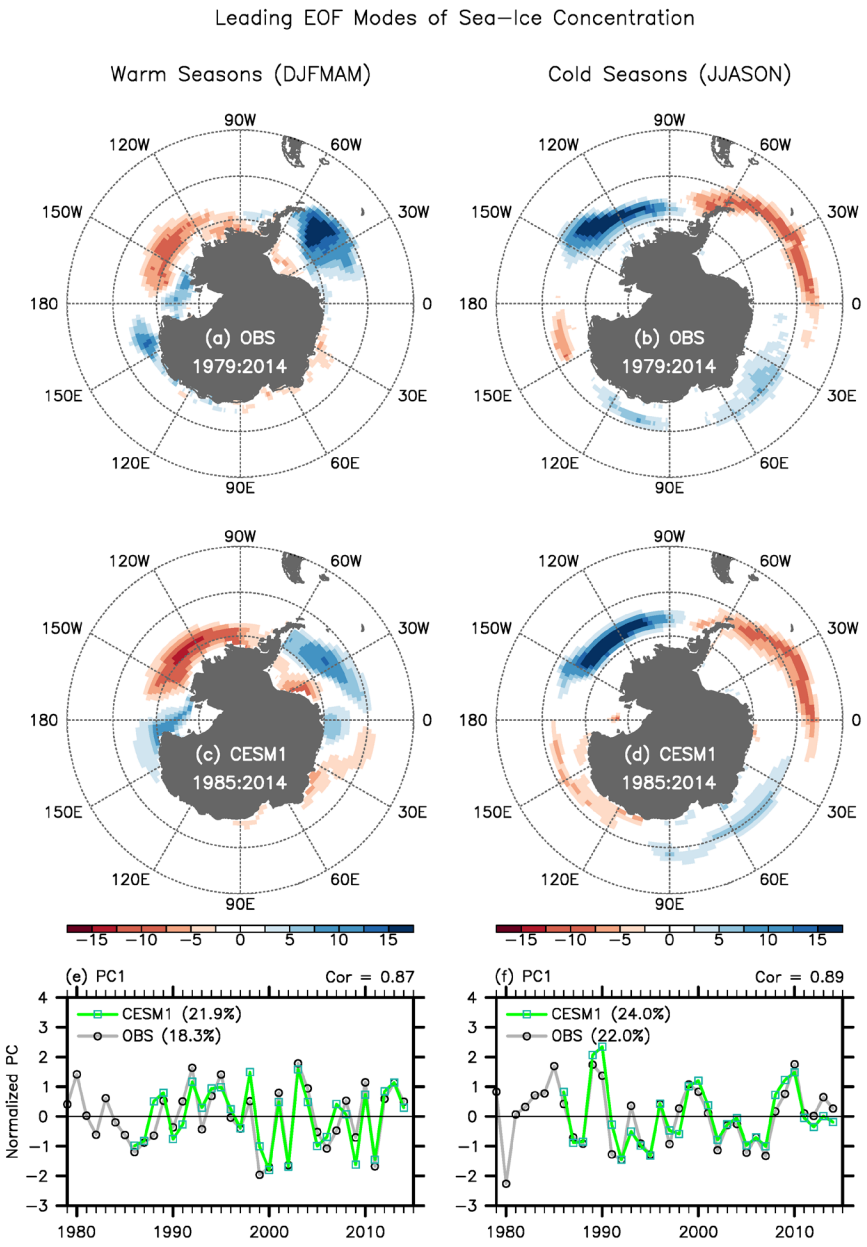

Figure 11. Leading Empirical Orthogonal Function (EOF) modes of detrended Antarctic sea-ice concentration variability during (a,c) the warm and (b,d) cold seasons, obtained from (a,b) the Hadley Center sea ice and sea surface temperature data sets over the period of 1979 - 2014 and (c,d) the historical simulation over the period of 1985 - 2014. The normalized principal components (PCs) of the leading modes are shown in (e,f). The percentage variance explained by each of the leading modes, and the correlations between the PCs derived from the observations and the historical simulation are indicated in (e,f). The units in (a-d) are % per two units of the normalized PCs.

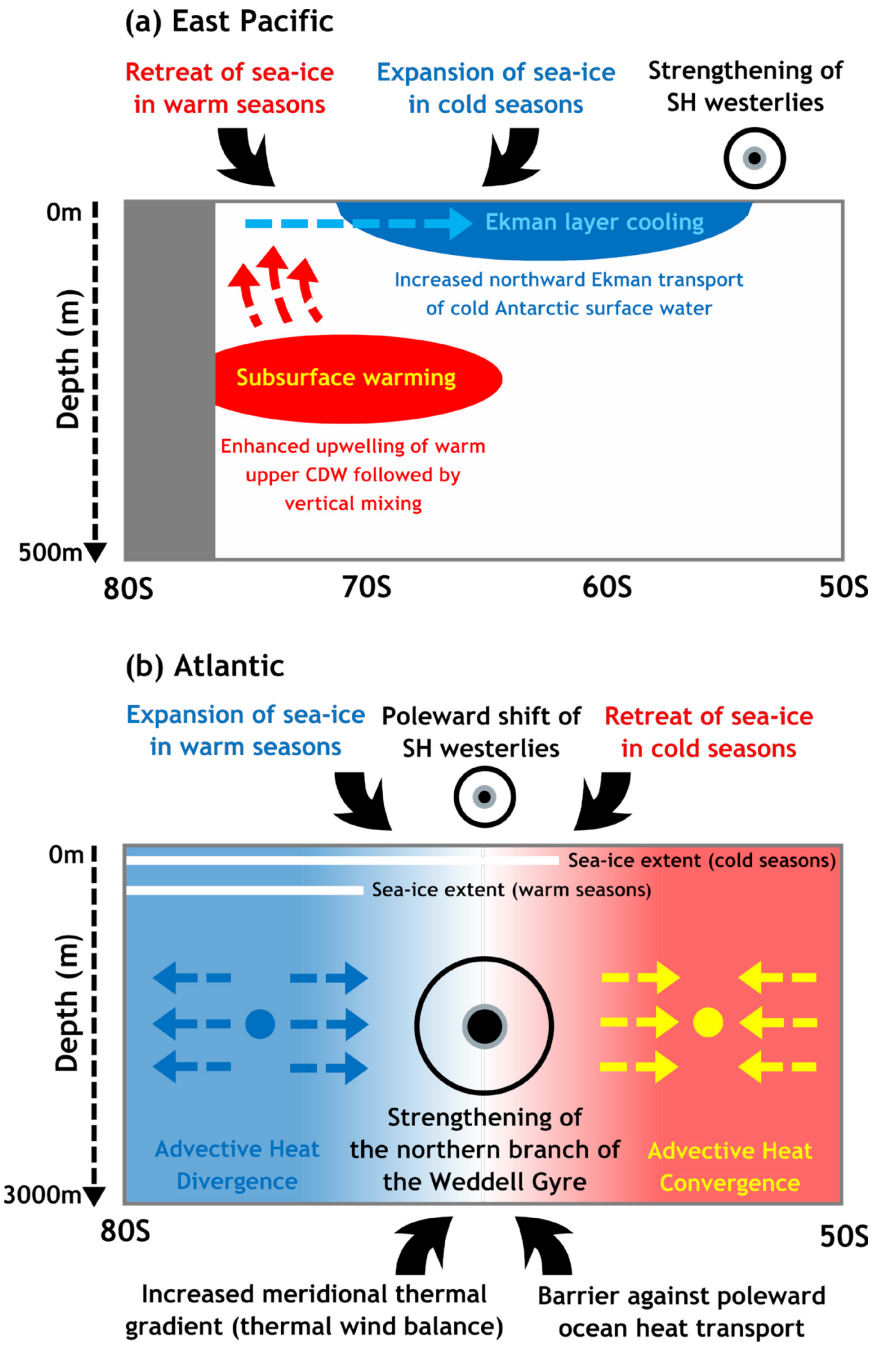

Figure 12. Sketch of the physical mechanisms linking the wind-driven ocean dynamics and the Antarctic sea-ice trends in (a) the East Pacific (150°W - 80°W) and (b) Atlantic (60°W - 0°) sectors. In the East Pacific sector, the strengthening SH westerlies enhanced Ekman upwelling of the warm upper CDW and increased the northward Ekman transport of cold Antarctic surface water, thus contributing to the expansion of sea-ice in the cold seasons and to the retreat in the warm seasons. In the Atlantic, the poleward shifting SH westerlies strengthened the northern branch of the Weddell Gyre. The strengthened the Weddell Gyre acted as a barrier against the poleward ocean heat transport, and thus produced anomalous heat divergence within the Weddell

Gyre and anomalous heat convergence north of the gyre. Hence, the meridional thermal gradient increased across the northern branch of the Weddell Gyre, as also constrained by the thermal wind balance, cooling the water column within the Weddell Gyre and warming the water column north of the gyre, thus contributing to the expansion of sea-ice in the warm seasons, and the retreat in the cold seasons.